# Weather Systems

# 8

With Lynn McMurdie and Robert A. Houze
Department of Atmospheric Sciences
University of Washington

The abundant rainfall that sustains life on Earth is not the bounty of cloud microphysical processes alone. Without vigorous and sustained motions, the atmospheric branch of the hydrological cycle would stagnate. Much of the ascent that drives the hydrologic cycle in the Earth's atmosphere occurs in association with *weather systems* with well-defined structures and life cycles. A small fraction of these systems achieve the status of *storms* capable of disrupting human activities and, in some instances, inflicting damage.

This chapter introduces the reader to the structure and underlying dynamics of weather systems and their associated weather phenomena. The first section is mainly concerned with large-scale extratropical weather systems (i.e., baroclinic waves and the associated *extratropical cyclones*) and their embedded mesoscale fronts. The second section discusses some of the effects of terrain on large-scale weather systems and some of the associated weather phenomena. The third section describes the modes of mesoscale organization of deep cumulus convection. The final section describes a special form of organization in which a mesoscale convective system acquires strong rotation. These so-called *tropical cyclones* tend to be tighter, more axially symmetric, and more intense than their extratropical counterparts.

## 8.1 Extratropical Cyclones

Extratropical cyclones assume a wide variety of forms, depending on factors such as the background flow in which they are embedded, the availability of moisture, and the characteristics of the underlying surface. This section shows how atmospheric data are analyzed to reveal the structure and evolution of these systems. To illustrate these analysis techniques, we present a case study of a system that brought strong winds and heavy precipitation to parts of the central United States. The particular cyclone system selected for this analysis was unusually intense, but it typifies many of the features of winter storms in middle and high latitudes. Plotting conventions for the synoptic charts that appear in this section are shown in Fig. 8.1. A brief history of synoptic charts and a description of how modern synoptic charts are constructed is presented in the Appendix to Chapter 8 on the book web site [CD].

### 8.1.1 An Overview

This subsection documents the large-scale structure of the developing cyclone, with emphasis on the 500-hPa height, sea-level pressure, 1000- to 500-hPa thickness (a measure of the mean temperature of the lower troposphere) and vertical velocity fields. The development of the storm is shown to be linked to the intensification of a baroclinic wave.

The hemispheric 500-hPa chart for midnight (00) universal time (UTC: time observed on the Greenwich meridian[1]) November 10, 1998 is shown in Fig. 8.2. At this time, the westerly "polar vortex" is split into two regional cyclonic vortices, one centered over Russia and the other centered over northern Canada. Separating the vortices are pair of *ridges*, where the geopotential height contours bulge poleward. One of the ridges protrudes over Alaska and

[1] At longitudes west of the Greenwich meridian local time (LT) lags universal time (UTC) by 1 h for each ~15° of longitude, less 1 h during daylight savings time. For example, in the United States, 00 UTC corresponds to 19 EST, 20 EDT, and 16 PST of the previous day.

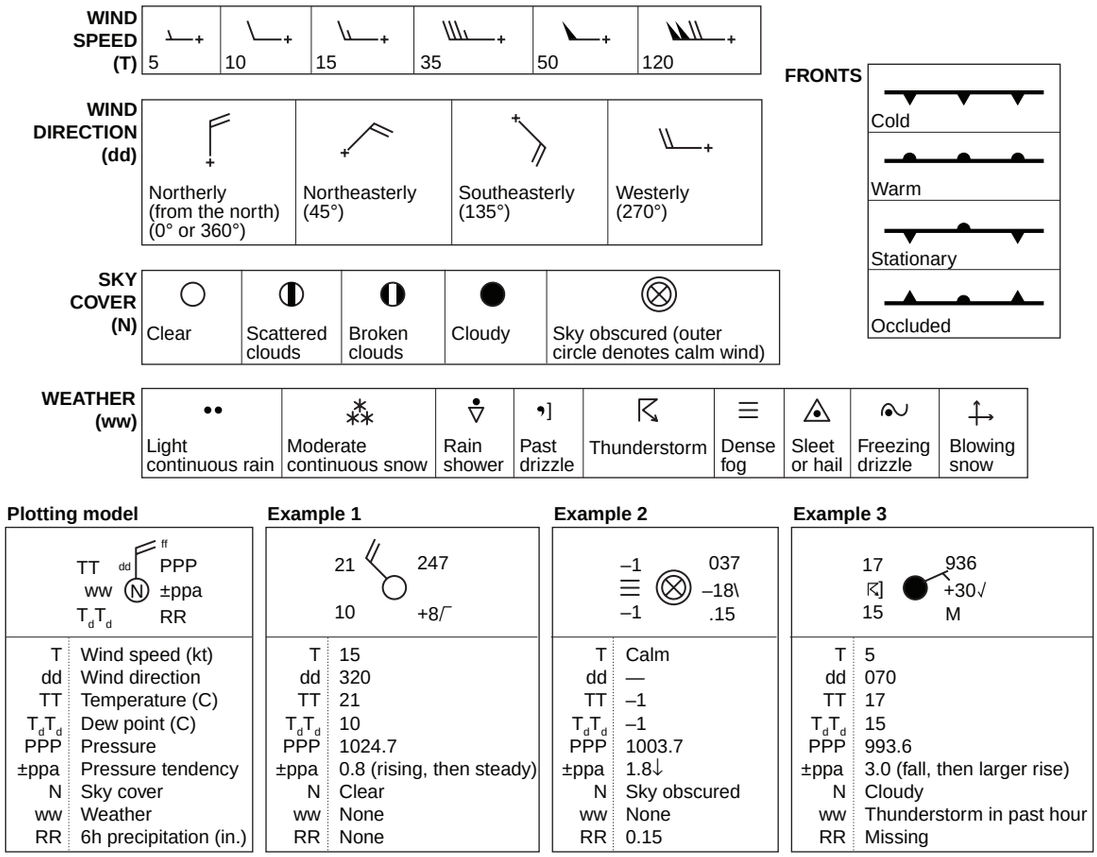


**Fig. 8.1** Plotting convections used in synoptic charts.

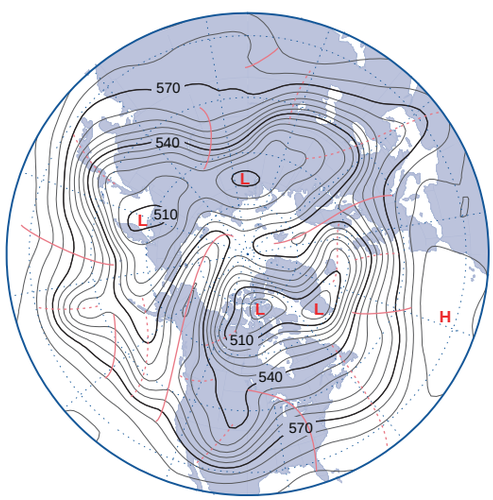


**Fig. 8.2** Hemispheric 500-hPa height chart for 00 UTC Nov. 10, 1998. Contours at 60-m intervals. Contours labeled in tens of meters (decameters, dkm). Solid red lines denote the axes of *ridges*, and dashed red lines denote the axes of *troughs* in the 500-hPa wave pattern. [Courtesy of Jennifer Adams, COLA/IGES.]

the other protrudes northward over Scandinavia. Pronounced *troughs* (along which the contours bulge equatorward) are evident over the Black Sea, Japan, the central Pacific, and the United States Great Plains, and several weaker troughs can be identified at other locations. The typical distance between successive troughs (counting the weaker ones) is ~50° of longitude or 4000 km, which corresponds to the theoretically predicted wavelength of baroclinic waves.

Time-lapse animations of weather charts like the one shown in Fig. 8.2 reveal that baroclinic waves move eastward at a rate of $\sim 10\ \mathrm{m\ s^{-1}}$, which corresponds to the wintertime climatological-mean zonal wind speed around the 700-hPa level. Since the strength of the westerlies generally increases with height within the extratropical troposphere, air parcels above this so-called *steering level* pass through the waves from west to east, while air parcels below that level are overtaken by the waves. Successive ridges (or troughs) typically pass a fixed point on Earth at intervals of roughly 4 days, but they may be only a day or two apart if the steering flow is very strong.

Lapses of a week or longer may occur between wave passages in the sectors of the hemisphere where the westerlies aloft are blocked by strong ridges. The direction of propagation tends to follow the steering flow, which nearly always exhibits a strong eastward component. Baroclinic waves are observed most regularly and tend to be strongest over the oceans, but they can develop over land, as in this case study. Baroclinic wave activity tends to be most vigorous during winter when the meridional temperature gradient across midlatitudes is strongest.

A more detailed view of the 500-hPa height pattern over the North American sector at 00 UTC November 10 is shown in Fig. 8.3, and the charts for

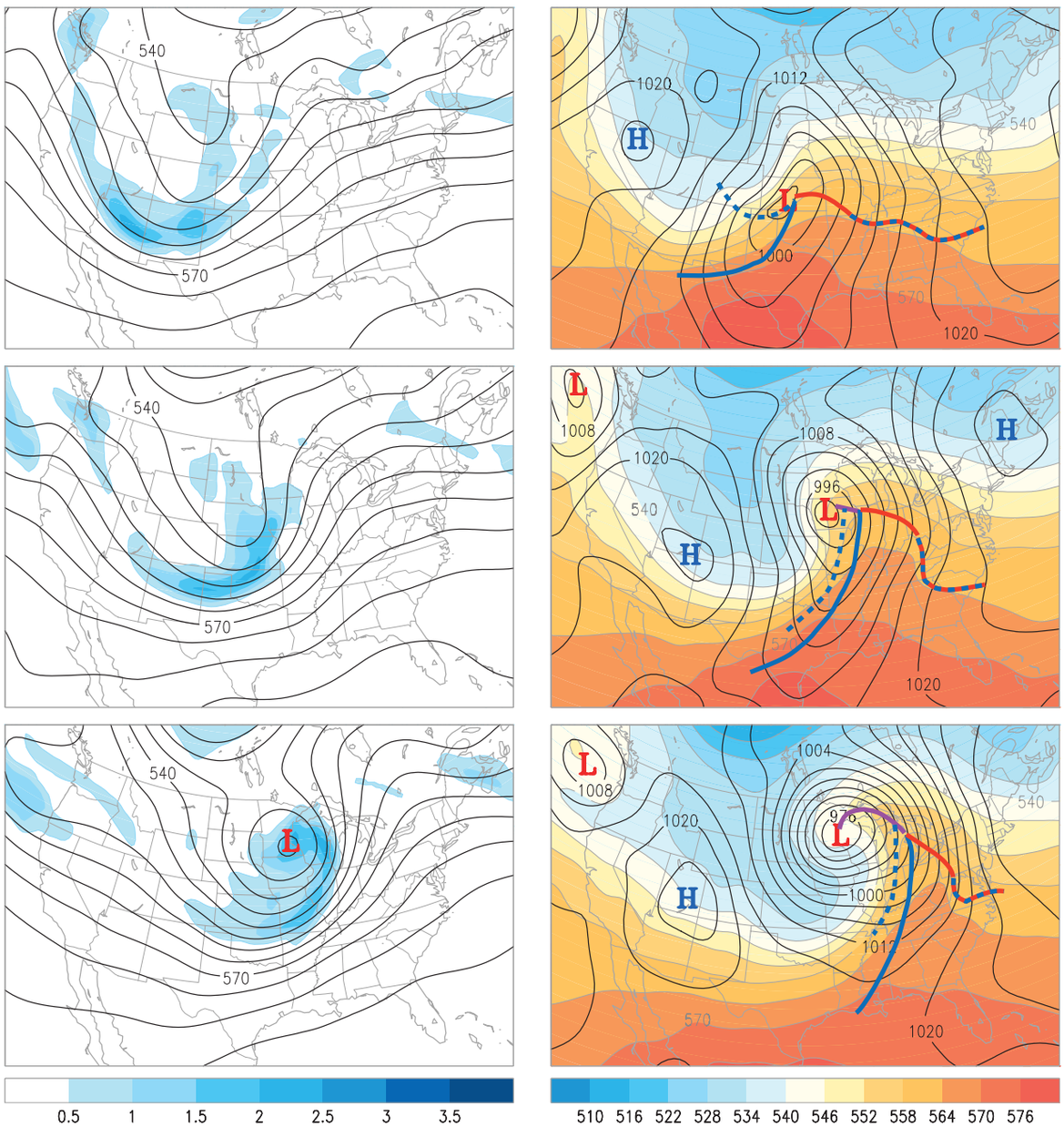


**Fig. 8.3** Synoptic charts at 00, 09, and 18 UTC Nov. 10, 1998. (Left) The 500-hPa height (contours at 60-m intervals; labels in dkm) and relative vorticity (blue shading; scale on color bar in units of $10^{-4}\,s^{-1}$). (Right) Sea-level pressure (contours at 4-hPa intervals) and 1000- to 500-hPa thickness (colored shading: contour interval 60 m; labels in dkm). Surface frontal positions, as defined by a skilled human analyst, are overlaid. [Courtesy of Jennifer Adams, COLA/IGES.]

9 and 18 h later are shown below it. Clearly evident in this three-chart sequence is the eastward propagation and intensification of the trough that passes over the United States Great Plains. In the third chart in the sequence, the base of this trough splits off from the westerlies to form a *cutoff low* (i.e., an isolated minimum in the geopotential height field), implying the existence of a closed cyclonic circulation. The dramatic intensification of the winds encircling this feature is reflected in the tightening of the spacing between adjacent 500-hPa height contours.

The intensification of the trough at the 500-hPa level is accompanied by the deepening of the corresponding low pressure center in sea-level pressure field, as shown in the right-hand panels of Fig. 8.3. This surface low marks the center of a closed cyclonic circulation referred to as an *extratropical cyclone*. Also evident in the right-hand panels of Fig. 8.3 is the amplification of the west-to-east gradient in the 1000- to 500-hPa thickness field, indicated by the colored shading. In the first chart of the sequence the developing surface low is located well to the east of the corresponding trough in the 500-hPa height field, but as these features amplify, they come into vertical alignment in subsequent charts of the sequence.

Now let us examine this sequence of events in greater detail. Embedded in the *long-wave trough* over western North America in the first chart in the sequence (Fig. 8.3, upper left panel) are several smaller scale features, which show up clearly in the vorticity field. The vorticity maxima along the coast of British Columbia and over northern Arizona correspond to *short-wave troughs*, in which the horizontal flow exhibits both cyclonic curvature and cyclonic shear. The shear is particularly strong in the Arizona trough. Nine hours later (Fig. 8.3, middle left panel) these vorticity maxima and their associated troughs appear downstream of their previous positions: the former is centered over the state of Washington and the latter has evolved into an elongated comma-shaped band trailing westward from Kansas, across the Texas Panhandle and into New Mexico. In the final chart of the sequence, the head of the comma-shaped feature is centered over southeastern Minnesota.

In the corresponding sequence of surface charts shown in the right-hand panel of Fig. 8.3, the central pressure of the surface low, as analyzed in Fig. 8.3, dropped from 998 hPa at 00 UTC Nov. 10 (top panel) to 978 hPa at 18 UTC (bottom panel), and 968 hPa at 00 UTC Nov. 11 (not shown), a deepening rate of 30 hPa per day, which is three times as rapid as observed in a typical extratropical cyclone. At 00 UTC Nov. 10 (Fig. 8.3, top panel) the center of the extratropical cyclone (as defined by the sea-level pressure field) was located ~1/4 wavelength downstream of the 500-hPa trough and just about directly underneath the jet stream. In contrast, in the last of the three charts the surface low was situated almost directly beneath the cutoff low in the 500-hPa height field, and on the poleward (cyclonic) side of the jet stream.

The top panel of Fig. 8.4 shows the same information for the same three map times, depicted in a slightly different way. In this case the geopotential height field at the Earth's surface is represented in terms of the geopotential height of the 1000-hPa surface. Contours of 1000-hPa height, 500-hPa height and 1000- to 500-hPa thickness are superimposed on the same set of charts, with the same (60-m) contour interval. The lower panels of Fig. 8.4 show the evolving structure of a typical baroclinic wave, as depicted in a synoptic meteorology textbook written over a generation ago. The high degree of correspondence between the real features observed in this case study and the idealized features in the textbook representation establishes that the case study presented in this section typifies many of the features of baroclinic waves.

The amplification of the wave in the thickness field is due to horizontal temperature advection by the cyclonic circulation around the deepening surface low. The southerly wind component to the east of the low advects warm air northward while the northerly component to the west of the low advects colder air southward. The strengthening of the east–west temperature contrasts in the lower tropospheric temperature field leads to a weakening of the north–south temperature gradient in the background field on which the wave is growing. As the surface low intensifies over the 9-h interval spanned by the first two charts, the winds around it strengthen while the angle between the geopotential height contours and the thickness contours increases, resulting in a dramatic increase in the horizontal temperature advection. However, in the later stage of development during the interval between the second and third charts, the surface low comes into alignment with the 500-hPa trough, and the 1000-hPa height, 500-hPa height, and 1000- to 500-hPa thickness contours come into alignment with each other, resulting in a weakening of the horizontal temperature advection. In the language

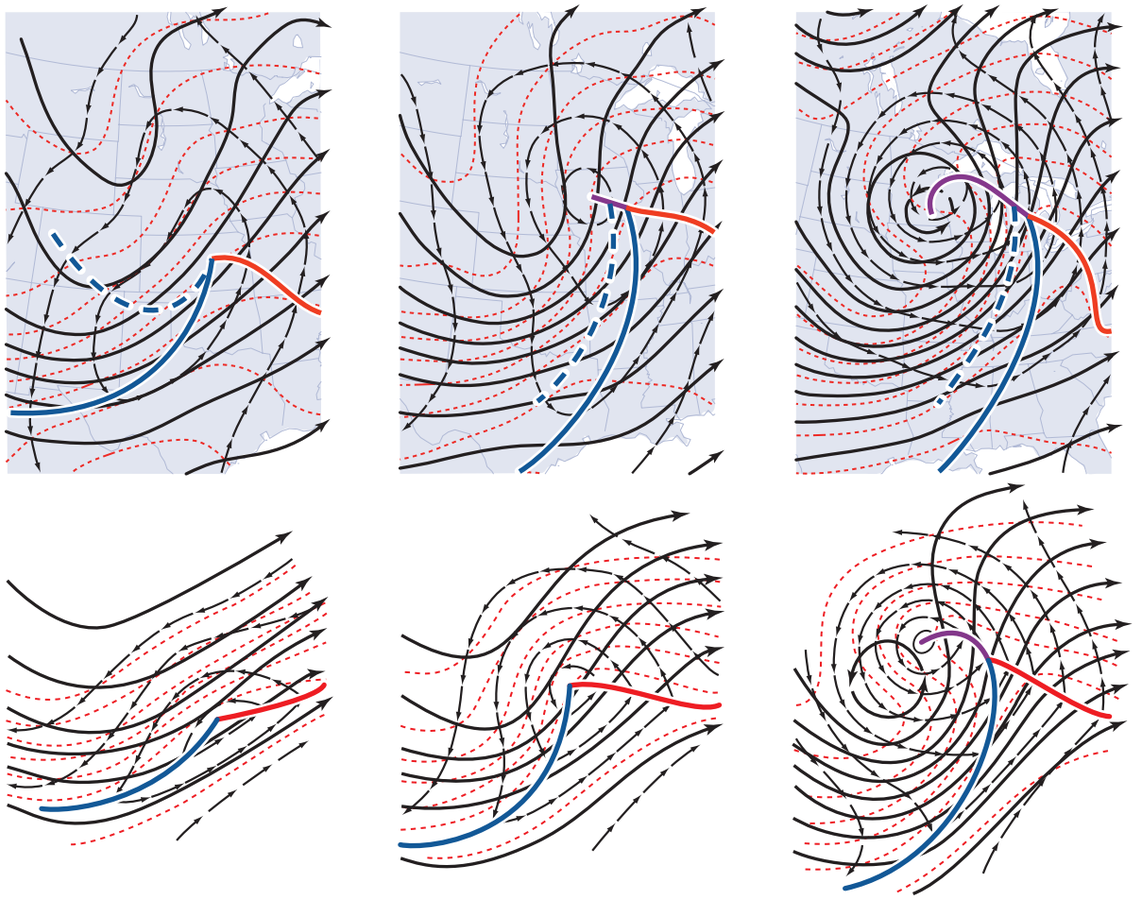

**Fig. 8.4** (Top) Fields of 500-hPa height (thick black contours) 1000-hPa height (thin black contours), and 1000- to 500-hPa thickness (dashed red) at 00, 09, and 18 UTC Nov. 10, 1998; contour interval 60 m for all three fields. Arrows indicate the sense of the geostrophic wind. (Bottom) Idealized depictions for a baroclinic wave and its attendant tropical extratropical cyclone in its early (left), developing (center), and mature (right) stages. [Top panel courtesy of Jennifer Adams, COLA/IGES. Bottom panel adapted from *Atmospheric Circulation Systems: Their Structure and Physical Interpretation*, E. Palmén and C.W. Newton, p. 326, Copyright (1969), with permission from Elsevier.]

introduced in Section 7.2.7, the geostrophic wind field evolves from a highly *baroclinic* pattern, with strong turning of the geostrophic wind with height in amplifying baroclinic waves, into a more *equivalent barotropic* pattern, with much less directional shear of the lower tropospheric geostrophic wind field in fully developed baroclinic waves. This transition from a highly baroclinic structure, with strong temperature contrasts in the vicinity of the surface low, to a more barotropic structure with strong winds but weaker temperature gradients, marks the end of the intensification phase in the life cycle of the cyclone.

The vertical velocity field also plays an important role in the development of baroclinic waves. Figure 8.5 shows the vertical velocity field superimposed on the 500-hPa height field. In the left panel, which corresponds to the time when the system is developing most rapidly, the northward moving air in the region of warm advection in advance of the developing surface low is rising, while the southward moving air in the region of cold advection to rear of the cyclone is sinking. It is also apparent from the right-hand panels of Fig. 8.3 that at any given latitude the rising air to the east of the surface low is warmer than the sinking air to the west of it. We recall from Section 7.4.1 that the rising of warm air and sinking of cold air is indicative of a conversion of potential energy into kinetic energy. In the case of baroclinic waves, the potential energy is associated with the east–west temperature gradients and the kinetic energy is primarily associated with the meridional wind component.

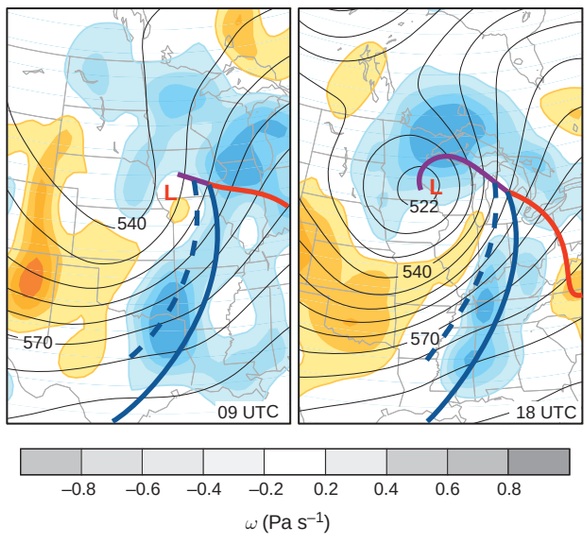


**Fig. 8.5** The 500-hPa height (in tens of meters) and vertical velocity (in Pa $s^{-1}$) fields at the 700-hPa level at 09 and 18 UTC Nov. 10, 1998. Blue shading (negative $\omega$) indicates ascent and tan shading indicates subsidence. [Courtesy of Jennifer Adams, COLA/IGES.]

In the right-hand panel of Fig. 8.5 warmer air to the east of the cyclone is still rising, but the region of ascent wraps around the northern and western flanks of the surface low. In a similar manner, the region of subsidence to the west wraps around the southern and eastern flanks of the cyclone. The juxtaposition of these inward-spiraling rising and subsiding air currents, reminiscent of the "yin-yang pattern" in Asian art, is influential in shaping the cloud and precipitation patterns associated with extratropical cyclones, as shown in the next subsection.

## 8.1.2 Fronts and Surface Weather

The previous subsection documented the broad outlines of an intense storm that developed over the north central United States. Much of the significant weather observed in association with such systems tends to be concentrated within narrow bands called *frontal zones*, which are marked by sharp horizontal gradients and sometimes by outright discontinuities in wind and temperature. The development of frontal zones (*frontogenesis*, in the vernacular) is initiated by the large-scale horizontal deformation field, as discussed in Section 7.1.3. Mesoscale circulations in the plane perpendicular to the fronts are instrumental in sharpening the temperature contrasts and in organizing the distribution of precipitation into bands oriented parallel to the fronts. This subsection documents the expressions of the November 10, 1998 storm and its attendant frontal zones in (a) wind and pressure, (b) temperature, (c) moisture variables, (d) surface weather, (e) the suite of hourly observations, (f) satellite imagery, and (g) radar imagery.

### *a. Wind and pressure*

Figure 8.6 shows the sea-level pressure and surface winds at 9-h intervals starting at 00 UTC Nov. 10 (note that the field of view is smaller than in the previous charts). At all three map times a pronounced wind-shift line, the expression of the *cold front* in the surface wind field, is evident to the south of the surface low. To the west of the cold front the surface winds exhibit a strong westerly component, whereas to the east of it the southerly wind component is dominant. The isobars bend sharply (and some change direction abruptly or "kink") along the front. Hence, as the front passes, a fixed observer at the Earth's surface would experience a veering (i.e., shifting in an anticyclonic sense) of the wind from southerly to westerly, concurrent with a well-defined minimum in sea-level pressure. Through the three-chart sequence the cold front advances eastward, keeping pace with and showing some tendency to wrap around the surface low as it deepens and tracks northeastward. It appears as though the front is being advected by the intensifying cyclonic circulation.

The wind-shift line extending eastward from the surface low, the expression of the *warm front*, is a more subtle feature, the reality of which becomes clearly evident when the surface charts are analyzed in conjunction with hourly station data, as illustrated later in this subsection. Like the cold front, the warm front shows indications of being advected around the developing surface low. When it passes a station the wind veers from southeasterly to southerly. In the later stages of the development of the cyclone, as represented in the 18 UTC panel in Fig. 8.6, the junction of the cold and warm fronts becomes separated from the center of the surface low and an *occluded front* extends from the center of the surface low to a *triple point* where it meets the junction of the warm and cold fronts. When the occluded front passes a station the surface wind veers from southeasterly to southwesterly.

A fourth wind-shift line, the expression of a *secondary cold front*, rendered in dashed blue, also appears on the charts for 00 and 09 UTC. In the 00 UTC chart the line curves eastward from the eastern

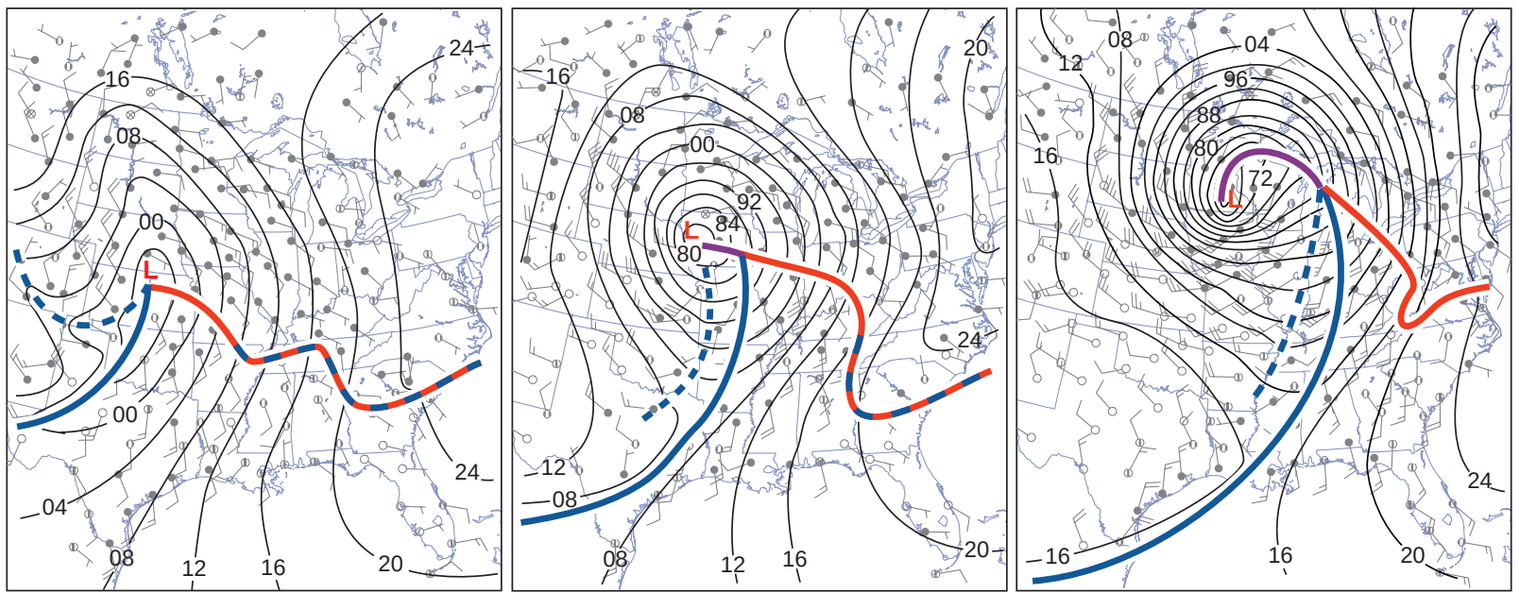


**Fig. 8.6** Sea-level pressure, surface winds and frontal positions at 00, 09, and 18 UTC 10 Nov. 1998. Frontal symbols and wind symbols are plotted in accordance with Fig. 8.1. The dashed blue line denotes the secondary cold front. In this figure and in subsequent figures in this section, the frontal positions are defined by a human analyst. The contour interval for sea-level pressure is 4 hPa. [Sea-level pressure and frontal analyses by Lynn McMurdie, figure Courtesy of Jennifer Adams, COLA/IGES.]

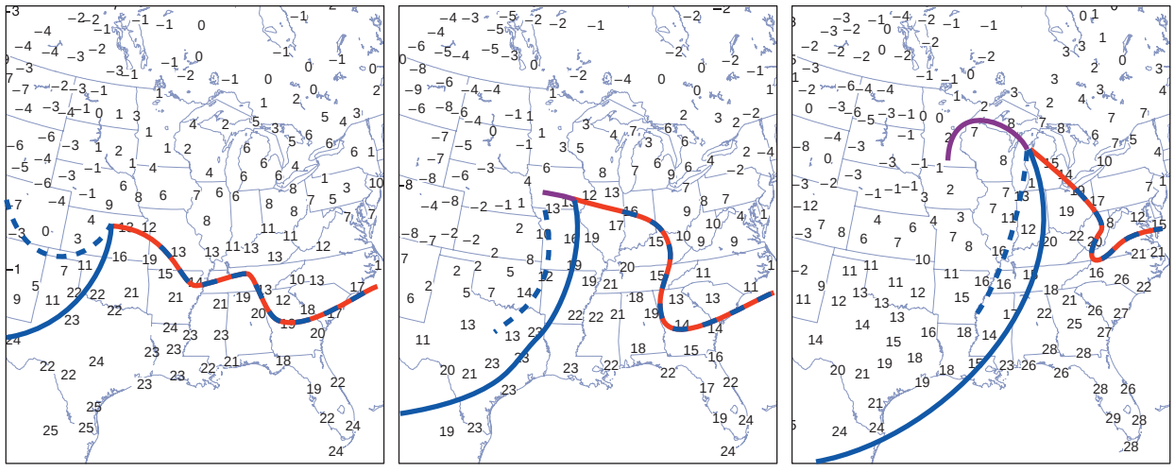

**Fig. 8.7** Surface air temperature (in °C) and frontal positions at 00, 09, and 18 UTC 10 Nov. 1998. [Courtesy of Jennifer Adams, COLA/IGES.]

slope of the Colorado Rockies and then northeastward into the center of the surface low. This feature is also embedded in a trough in the sea-level pressure field and causes the surface wind at a fixed station to veer when it passes.

### *b. Temperature*

Figure 8.7 shows the surface air temperatures at the same three map times. The field is represented by raw station data rather than by isotherms, and the positions of the fronts are transcribed from the previous figure. In the southerly flow off the Gulf of Mexico to the east of the cold front, temperatures are relatively uniform, with values in excess of 20 °C extending as far northward as southern Illinois at 09 UTC and values in the teens as far northward as the Great Lakes at 18 UTC. This zone of relatively uniform temperature to the southeast of the surface low is referred to as the *warm sector* of a cyclone. The cold front marks the leading edge of the advancing colder air from the west. In this system, the cold front is not a zero-order discontinuity in the temperature field (i.e., a discontinuity of the temperature itself), but a first-order discontinuity (i.e., a discontinuity in the horizontal temperature gradient). To the east of the cold front the temperatures are relatively homogeneous, while proceeding westward from the front, temperatures drop by 10 °C or more within the first few hundred kilometers. Hence, a cold front can be defined as the warm-air boundary of a *frontal zone* (or *baroclinic zone*) that is advancing in the direction of the warmer air. The passage of a cold front at a station marks the beginning of a period of falling temperatures, heralded by a wind shift.

The November 10, 1998 storm had two cold fronts: a *primary cold front* at the warm air boundary of the frontal zone and a *secondary cold front* within the frontal zone. The two cold fronts show up clearly in the zoomed-in chart for 00 UTC, Nov. 10, 1998, shown in Fig. 8.8. Both fronts are embedded within

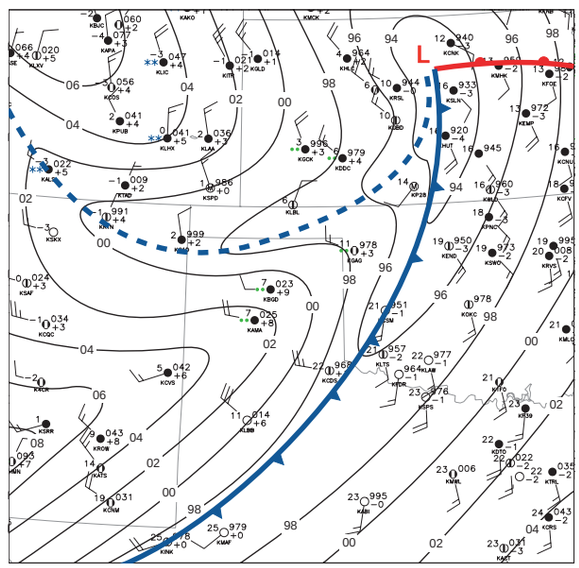

**Fig. 8.8** Close-up of surface weather conditions over the southern United States Great Plains at 00 UTC Nov. 10, 1998, showing data plotted using the conventional station model illustrated in Fig. 8.1. [Courtesy of Lynn McMurdie.]

troughs of low pressure and their passage is marked by wind shifts. The passage of the primary cold front marks the onset of the cooling and the passage of the secondary front marks the beginning of an interval of renewed cooling. The secondary cold front marks the leading edge of a band of enhanced baroclinicity (i.e., temperature gradient) within the more broadly defined frontal zone. The passage of such a front marks the onset of renewed cooling.

The more subtle warm front in Fig. 8.7 also marks the warm-air boundary of a baroclinic zone, but in this case the baroclinic zone is advancing northward, displacing the colder air. The passage of a warm front at a fixed station thus is preceded by an interval of rising temperatures. Fronts that exhibit little movement in either direction are labeled as *stationary fronts* and are indicated on synoptic charts as dashed lines with alternating red and blue line segments, as in Figs. 8.6 and 8.7.

From an inspection of Fig. 8.4 it is evident that in the early stages of cyclone development, the cold and warm fronts mark the warm air boundary of the same, continuous baroclinic zone. The cyclone develops along the warm air boundary of the frontal zone, but it subsequently moves away from it, in the direction of the colder air. As this transition occurs, air from within the frontal zone wraps around the cyclone forming the occluded front. It is apparent from Fig. 8.7 that as the occluded front, rendered in purple, approaches a station, surface air temperature rises, and after the front passes the station, the temperature drops. From the standpoint of a stationary observer, experiencing the passage of an occluded front is like experiencing the passage of back-to-back warm and cold fronts except that the temperature changes are usually more subtle because the observer does not experience temperatures as high as those in the warm sector.

Fronts on surface maps are expressions of frontal surfaces that extend upward to a height of several kilometers, sloping backward toward the colder air. Regardless which way the front is moving, air converges toward the front at low levels and the warmer air tends to be lifted up and over the frontal surface along sloping trajectories, as depicted in Fig. 8.9. In the case of a stationary front, warm air may be advancing aloft while the frontal zone air trapped beneath the frontal surface remains stationary. In the case of a cold front, the wind component normal to the front may be in the opposite direction below and above the frontal surface.

Fronts are sometimes pictured as material surfaces, separating air masses characterized by different temperatures and/or humidities, that move about passively in the atmosphere, advected by the winds. This simplistic description ignores the important role of dynamical processes in forming and maintaining fronts. The formation of fronts, a process referred to as *frontogenesis*, involves two-steps. In the first step, the broad, diffuse equator-to-pole temperature gradient tends to be concentrated into frontal zones hundreds of kilometers in width by the large-scale deformation field, as discussed in Section 7.1.3. In the second step, transverse circulations, like those depicted in Fig. 8.9, collapse the low-level temperature gradients within preexisting, still relatively broad frontal zones, down to a scale of tens of kilometers or less.

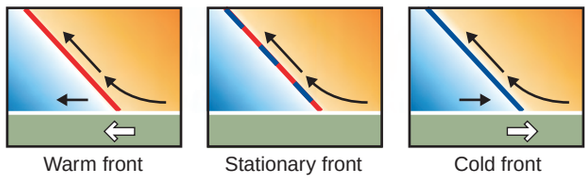


**Fig. 8.9** Idealized cross sections through frontal zones showing air motions relative to the ground in the plane transverse to the front. Colored shading indicates the departure of the local temperature from the mean temperature of the air at the same level. (a) Warm front, (b) stationary front with overrunning warm air, and (c) cold front. Heavy arrows at the bottom indicate the sense of the frontal movements.

Lest the role of fronts in mediating surface air temperature be overemphasized, it should be noted that other factors such as time of day, sky cover, altitude of the station, and proximity to large bodies of water can, at times, exert an equally important influence on the temperature pattern. In fact, it is sometimes difficult to locate fronts on the basis of gradients of surface air temperature because

- Over the oceans, surface air temperature is strongly influenced by the temperature of the underlying water, especially in regions where the atmospheric boundary layer is stably stratified.
- In mountainous terrain, large differences in station elevation mask the temperature gradients on horizontal surfaces.
- Unresolved features such as terrain effects, patchy nocturnal inversions, convective storms, and urban heat island effects can raise or lower the temperature at a given station by several degrees relative to that at neighboring stations. Apparent temperature discontinuities associated with these features are sometimes misinterpreted as fronts.

### c. Moisture

Frontal zones also tend to be marked by strong gradients in dew point and equivalent potential temperature, especially when the cold air is of continental origin and the warmer air is of marine origin, as is often the case over the eastern United States. In the case study considered in this section, the distributions of temperature and dew point are generally similar. However, during spring and summer, the moisture gradient is often a more reliable indicator of frontal positions than the gradient of surface air temperature because it is less subject to the confounding influence of diurnal variability. For example, during summer over land, the diurnal temperature range at the ground tends to be larger in cool, dry continental air masses than in warm, humid air from off the Gulf of Mexico. Thus, during afternoon it is not uncommon for surface temperatures well behind the cold front to be as high as those on the warm sector of the cyclone, even though there is considerable thermal contrast 1–2 km above the ground. In such situations, the front is more clearly defined in the dew point field than in the temperature field.

Land–sea geometry and terrain features can sometimes give rise to fronts in the moisture field that have no direct relation to extratropical cyclones. For example, during summer, under conditions of southerly low level flow, there often exists a sharp contrast between humid air advected northward from the Gulf of Mexico and much drier air that has subsided along the eastern slopes of the Rockies. The boundary between these marine and continental air masses is referred to as the *dry line*.

### d. Hourly observations

Now let us look at the expressions of fronts in hourly surface observations. Hourly pressure, surface wind, temperature, and dew point observations for Gage, Oklahoma, shown in Fig. 8.10, confirm the passage of the primary cold front at 22 UTC (16 LT) Nov. 9, as evidenced by the strong veering of the wind and the onset of an interval of falling temperature and rising sea-level pressure. The passage of the secondary cold front occurred around 03 UTC Nov. 10, when the wind veered and strengthened, the sea-level pressure exhibited a weak minimum, and temperature and dew point began to drop more sharply after having nearly leveled off for several hours.

The time series for Bowling Green, Kentucky, shown in Fig. 8.11, are indicative of a well-defined warm frontal passage around 05 UTC (23 LT), with a

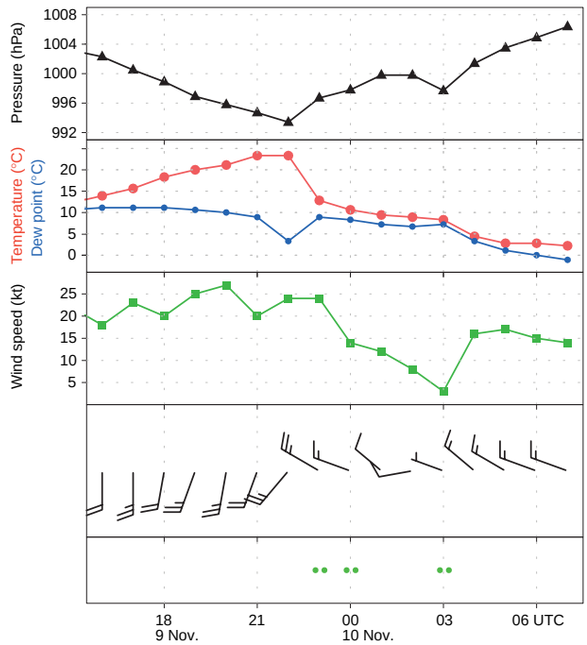


**Fig. 8.10** Hourly surface observations at Gage, Oklahoma (KGAG in Fig. 8.36) showing the passage of the primary and secondary cold fronts. The locations of Gage and the other stations for which time series of hourly station observations are shown are indicated in Fig. 8.36 at the end of Section 8.2. [Courtesy of Jennifer Adams, COLA/IGES.]

wind shift from easterly to southerly and a leveling off of the dew point after a prolonged rise. Surface air temperature leveled off an hour later. Pressure continued to drop due to the approach and deepening of the surface low, but the rate of change was smaller than it had been prior to the passage of the front.

As the storm moved northeastward the band of strongest *baroclinicity* (i.e., horizontal temperature gradient) shifted northward into the Great Lakes and the warm front became less distinct. To the east of the Appalachian mountain range the advance of the warm air was delayed by a persistent, topographically induced easterly flow, evident at several of the stations in Fig. 8.6, which advected cooler air southward through the Carolinas and Georgia. By 18 UTC (Fig. 8.6 right panel) the intensifying southerly winds in advance of the approaching cold front scoured out this colder air, resulting in an abrupt northward shift of the warm front at the Earth's surface. Time series of surface variables at Columbia, South Carolina, on the eastern side of the Appalachians (Fig. 8.12) show the warm frontal passage around 16 UTC (11 LT), which was marked by a wind shift and a rapid rise in temperature and dew point. On the west side of the

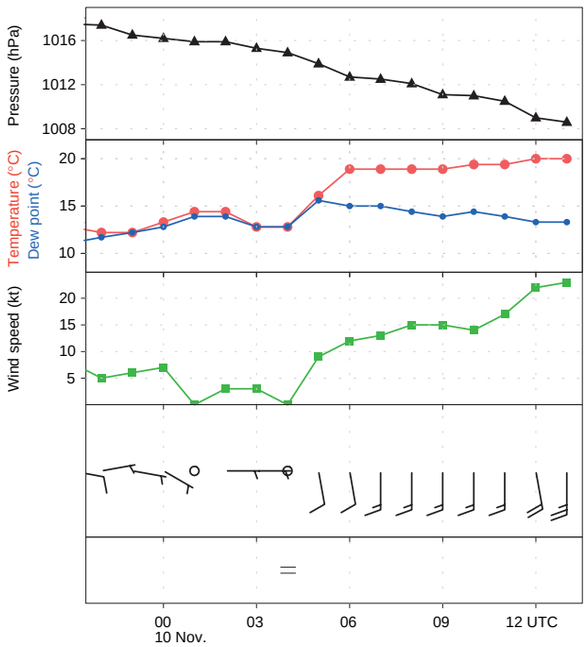


**Fig. 8.11** Hourly surface observations at Bowling Green, Kentucky (KBWG in Fig. 8.36) showing the passage of the warm front. [Courtesy of Jennifer Adams, COLA/IGES.]

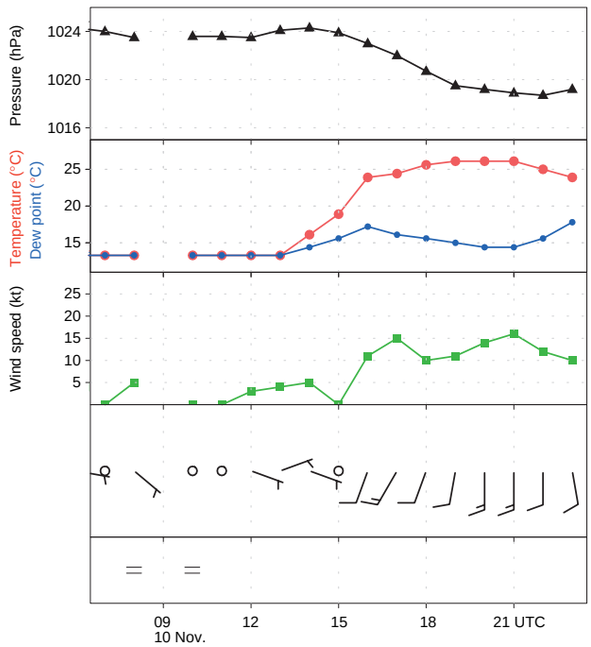


**Fig. 8.12** Hourly surface observations at Columbia, South Carolina (KCAE in Fig. 8.36) showing the delayed passage of the warm front. [Courtesy of Jennifer Adams, COLA/IGES.]

Appalachians the northward advance of the warm air occurred 12–18 h earlier.

The time series for Marquette, Michigan (Fig. 8.13) provides an example of the passage of an occluded front. The frontal passage, which occurred around 20 UTC Nov. 20 was attended by a leveling off of the pressure after reaching a remarkably low value of 975 hPa, an abrupt transition from rising to falling temperatures, and a more gradual veering of the wind, from southeasterly to southwesterly. Precipitation ended 3 h before the passage of the front and resumed, in the form of snow showers, 3 h after the frontal passage.

The movement and deepening of the surface low and the advance of the fronts are clearly evident in charts of the 3-h pressure tendency. The example shown in Fig. 8.14 is for the 3-h ending 09 UTC Nov. 10, the time of the middle chart in Figs. 8.6 and 8.7. The falling pressure centered over Iowa reflects both the approach and the deepening of the surface low. The pressure rises behind the cold front reflect the higher density of the colder air that was advancing into territory that was formerly a part of the warm sector of the cyclone. The pressure was falling rapidly ahead of the occluded front, while the pressure was steady behind it, the rising tendency induced by low level cold advection nearly

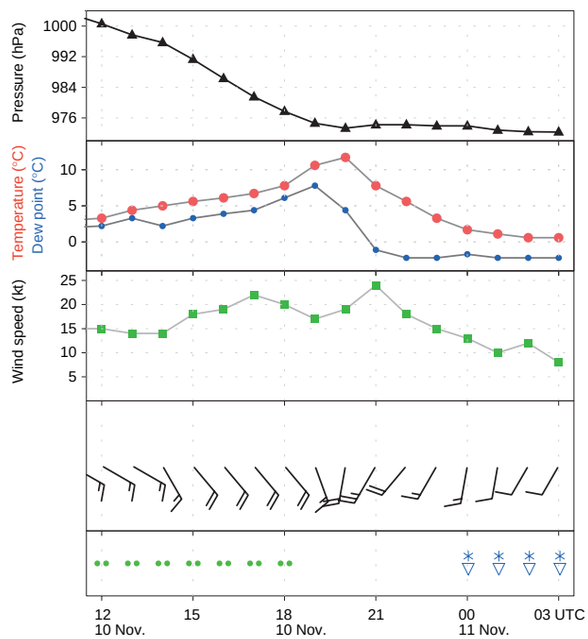


**Fig. 8.13** Hourly surface observations at Marquette, Michigan (KMQT in Fig. 8.36) showing the passage of the occluded front. [Courtesy of Jennifer Adams, COLA/IGES.]

balanced by the falling tendency induced by the deepening of the low as it passed to the northwest of the station.

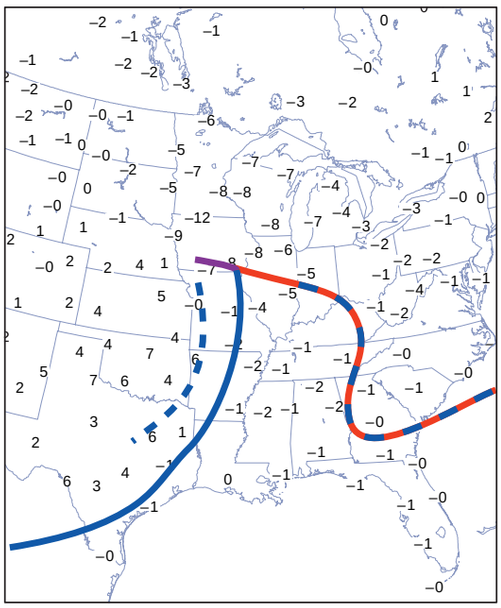

**Fig. 8.14** Sea-level pressure tendency (in hPa) for the 3-h interval ending 09 UTC Nov. 10, 1998. Heavy lines denote the frontal positions at this time. [Courtesy of Jennifer Adams, COLA/IGES.]

### *e. Surface weather*

The November 10, 1998 storm produced memorable weather over many parts of the central United States. Figure 8.15 shows the distribution of rain, snow, fog, and thunderstorms at the same times as the charts in Figs. 8.6 and 8.7. At 00 UTC (~18 LT), precipitation was already widespread in the northeast quadrant of the storm, with snow to the north and west and rain to the east and south. With few exceptions, precipitation was light at this time. Many stations to the north of the warm front were reporting fog.

At 09 UTC (03 LT; Fig. 8.15, middle), many of the stations in the Great Lakes region were reporting moderate to heavy rain. Snow reported in southern Minnesota at 00 UTC had changed to rain, reflecting the northwestward advance of the warmer air in the northeast quadrant of the storm, and the approach of the occluded front. The intensity of the snowfall over the Dakotas had increased and rain had changed to snow in eastern Nebraska. With nighttime cooling, fog had become more widespread in the region of the cold air damming over the Carolinas. Although it is not apparent on this map, several of the stations in Illinois and Indiana that reported rain earlier in the evening experienced intermittent fog later in the night, indicative of the passage of the warm frontal zone. Relative to 9 h earlier, more stations along and just behind the cold front were reporting rain at this time.

At 18 UTC (noon LT; Fig. 8.15, right), moderate to heavy snow was falling across much of the northern Great Plains, accompanied by strong winds. Hourly data for Sioux Falls, South Dakota, shown in Fig. 8.16 document blizzard-like conditions prevailing throughout most of the day. Many of the stations farther to the east along the advancing cold front experienced thunderstorms. Although heavy rain continued to be reported at many stations, the broad current of subsiding air circulating around the southern flank of the cyclone (Fig. 8.5) is reflected in the termination of precipitation over Illinois and much of Wisconsin. Marquette, Michigan (Fig. 8.13) experienced a 6-h lapse in precipitation beginning at 18 UTC.

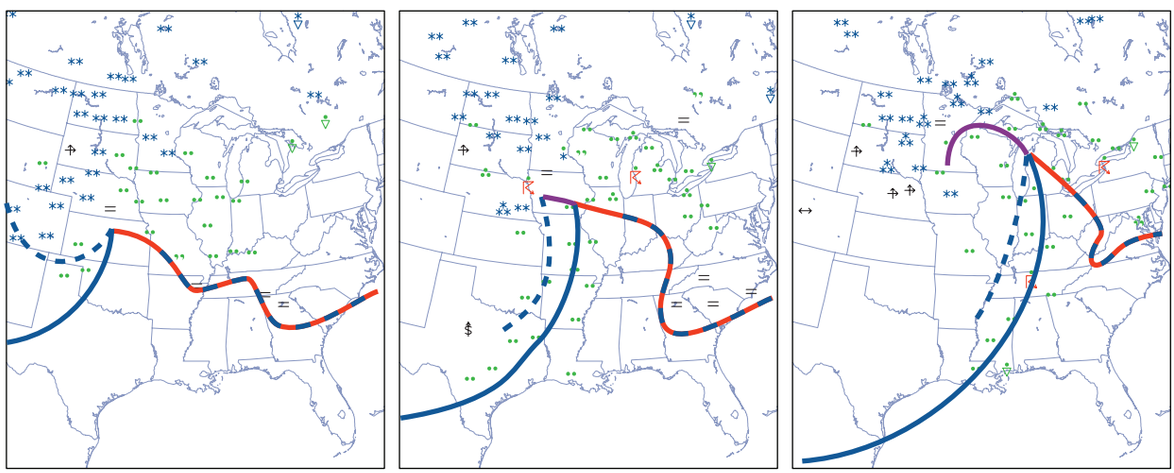

**Fig. 8.15** Surface weather observations of rain, snow, fog, and thunderstorms at 00, 09, and 18 UTC 10 Nov. 1998. For plotting conventions see Fig. 8.1. [Courtesy of Jennifer Adams, COLA/IGES.]

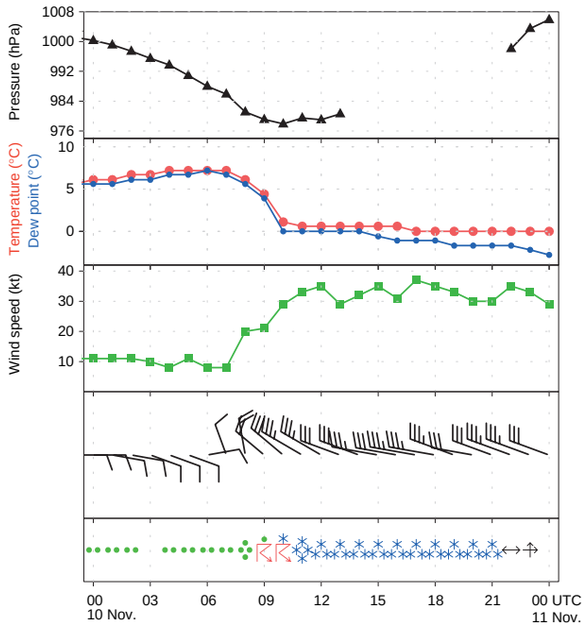


**Fig. 8.16** Hourly surface observations for Sioux Falls, South Dakota (KSUX in Fig. 8.36) just to the west of the track of the center of the surface low. Some of the pressure data are missing. [Courtesy of Jennifer Adams, COLA/IGES.]

### *f. Satellite imagery*

Infrared satellite imagery shown in Fig. 8.17 provides a large-scale context for the station observations shown in the previous figures. The first image (0015 UTC) shows a band of clouds with relatively cold tops that accounts for the (mostly light) rain and snow that was falling in the northeastern part of the storm. The warm front at this time corresponds fairly closely to the ragged southern edge of this rain band. Bowling Green, Kentucky, which experienced the passage of the front just a few hours later (Fig. 8.11), was not experiencing rain at this time, but it was located close to the patch of cold cloud tops along the southeastern edge of the band. The narrower and somewhat more coherent band emanating from the cold frontal zone over the Texas Panhandle and extending northward toward the Dakotas was evidently responsible for the light rain at stations in the Texas Panhandle (Figs. 8.8 and 8.15) and Gage, Oklahoma (Fig. 8.10), that was occurring around this time. The well-defined leading edge of this band, which appears as a narrow white line over Texas and as a thin yellow band over Oklahoma, widening into a blue and red "head" near the position of the surface low in Kansas, marks the position of the primary cold front. The patch of colder cloud tops in the northern segment of this band is the embodiment of a broad current of rising air streaming northward above the cold front and wrapping around the developing cyclone to form a comma-shaped "head." It is evident from time-lapse imagery that much of the structure within this air stream can be identified with the spreading of the "anvils" of convective clouds. Over the Texas Panhandle, where the convection along the cold front was shallow at this time, deeper clouds with an associated band of light rain were located, not along the front, but within the frontal zone around 150 km to the northwest of the primary cold front. Hence, these stations experienced

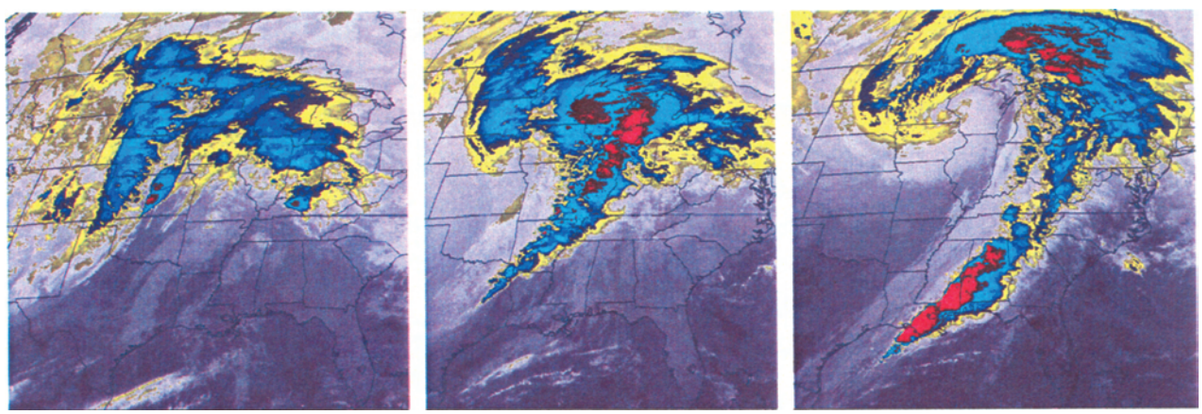

**Fig. 8.17** Infrared satellite imagery for 00, 09, and 18 UTC Nov. 10, 1998, based on radiation in the 10.7-$\mu$m channel, in which the atmosphere is relatively transparent in the absence of clouds. Radiances, indicative of equivalent black-body temperatures $T_E$ of the Earth's surface or the cloud top, are rendered on a scale ranging from black for the highest values (indicative of cloud-free conditions and a warm surface) with progressively lighter shades of gray indicative of lower temperatures and higher cloud tops. Color is used to enhance the prominence of the coldest (highest) cloud tops in the image.

a period of rain that began a few hours after the frontal passage.

At the time of the second image (09 UTC, Fig. 8.17, middle) the irregularly shaped cloud mass in advance of the warm front has moved northeastward into the southern Great Lakes and has assumed a "comma shape" as it wraps around the northern flank of the intensifying cyclone. The expansion of the area of blue shading over the Dakotas and Nebraska in the "head" of the comma is indicative of a thickening of the cloud deck over that region, consistent with the increase in the rate of snowfall from 00 to 09 UTC (Figs. 8.15 and 8.16). Stations in Illinois and Indiana that were under the cloud deck in the warm frontal zone and experiencing rain at 00 UTC were free of middle and high clouds at 09 UTC, with the clearing coinciding roughly with the passage of the warm front. An important aspect of the development of the cloud pattern in the interval from 00 to the 09 UTC is the pronounced lowering of the cloud top temperatures along the leading edge of the cold frontal cloud band, indicative of the deepening of the convection. As was the case at 00 UTC, this feature coincides with the primary cold front. The remnants of the cloud band that was over the Texas Panhandle at 00 UTC have become aligned with the secondary cold front.

In the final image in Fig. 8.17 at 18 UTC, the "yin-yang" signature in the vertical velocity field (Fig. 8.5, right panel) is clearly evident. The streamer of clouds emanating from the band of convection along the cold front curves cyclonically around the north side of the (now fully developed) cyclone and spirals inward around its western flank, where heavy snow is falling at this time.[2] Meanwhile, the equally pronounced current of darker-shaded subsiding air is wrapping around the southern flank of the cyclone, bringing an end to the precipitation in the areas immediately to the south and east of it. Remnants of the warm frontal cloud band can still be seen advancing northeastward ahead of the system, but they are becoming increasingly detached from the circulation around the cyclone.

Satellite imagery for the water vapor channel, shown in Fig. 8.18, yields additional insights into the structure and evolution of this remarkable storm. At 00 UTC (left) the deep convective clouds in the northern segment of the line of convection along the primary cold front over Kansas are clearly evident. In this respect, this image and the image from the

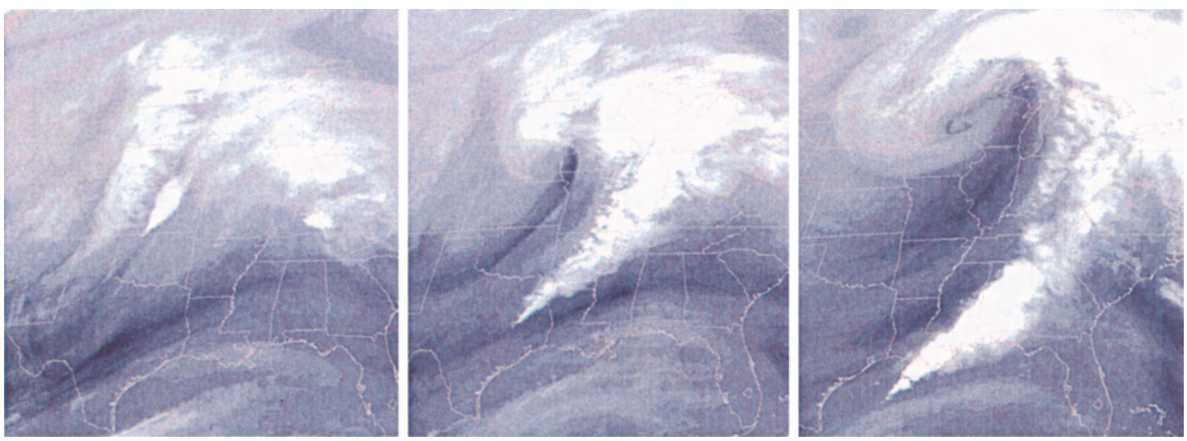

**Fig. 8.18** Satellite imagery for 00, 19 and 18 UTC Nov. 10, 1998, based on the 6.7 $\mu$m "water vapor channel." The radiances in this band provide a measure of the mid- and upper tropospheric humidity which, in turn, is determined by the air trajectories. Air that has been rising tends to be moist, resulting in a high optical depth, a low equivalent blackbody temperature and a low radiance, and vice versa. Low radiances, indicative of ascent are rendered by the lighter gray shades and high radiances, indicative of subsidence, by the darker shades. The brightest features in the images are clouds with high, cold tops.

[2] The fabled "nor'easters" that bury the eastern seaboard of the United States in half-meter-deep snow from time to time exhibit a structure much like this storm, with the heaviest snowfall in the northwest quadrant of the cyclone. Snowfall tends to be heavier in the coastal storms than in the storm examined in this chapter because much of the ascending air originates over the warm surface waters of the Gulf Stream (Fig. 2.5) where dew points are near 20 °C. The biggest snow producers are storms that slow down or execute tight cyclonic loops during the wrapping-up (or *occlusion*) process, thereby prolonging the interval of heavy snowfall. For an in-depth discussion of nor'easters, see P. J. Kocin and L. W. Uccellini, *Northeast Snowstorms*, Amer. Meteorol. Soc. (2004).

10.7-$\mu$m channel, shown in the previous figure, are similar. However, as one follows the front southward through Oklahoma and into Texas, the shallower clouds are masked by the overlying water vapor distribution, which is indicative of a narrow band of subsiding air almost directly above the front.

A prominent feature in the water imagery for the water vapor channel is the so-called *dry slot*, which first becomes apparent in the 09 UTC image and subsequently expands as it wraps around the cyclone. In some storm systems the dry slot is much more prominent in the imagery for the water vapor channel than in that for the 10.7-$\mu$m channel. The light gray shading over the Gulf of Mexico is indicative of a deep layer of moist, subtropical air that becomes entrained into the storm as it develops, fueling deep convection along the cold front.

### g. Radar imagery

Composite radar imagery shown in Figs. 8.19 and 8.21 confirms the existence of a narrow, persistent band of deep convection, a feature commonly referred to as a *squall line*, which, in this storm, is coincident with the advancing cold front.[3] Rainfall rates are heaviest along the leading edge of the line and trail off gradually behind it. Figure 8.20 shows hourly surface reports for Springfield, Missouri,

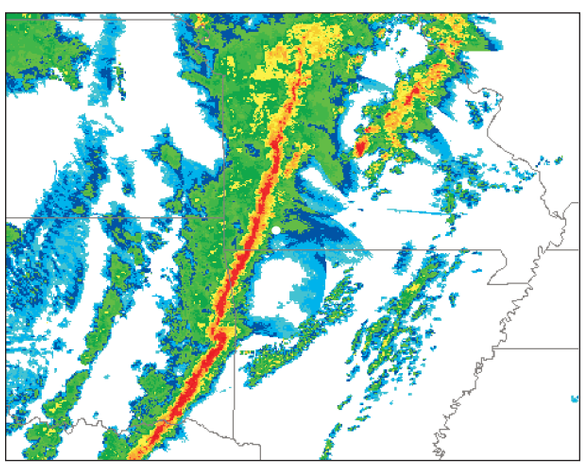

**Fig. 8.19** Composite radar image for 0620 UTC Nov. 10, 1998. Estimated rainfall rates increase by about a factor of five from the faintest echoes, rendered in blue, to the strongest echoes, rendered in red. The white circle indicates the location of Springfield, Missouri.

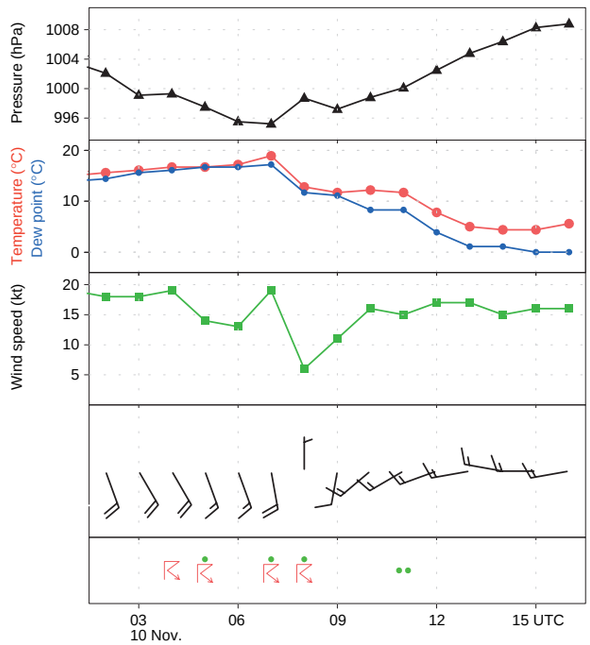


**Fig. 8.20** Hourly surface reports for Springfield, Missouri (KSGF in Fig. 8.36) showing the passage of the squall line and primary cold front around 07–08 UTC. [Courtesy of Jennifer Adams, COLA/IGES.]

located just to the east of the position of the squall line at 0620 UTC, the time of Fig. 8.19. Springfield reported thunder at 04 and 05 UTC and then again at 07 and 08 UTC. The later event marks the passage of the squall line in Fig. 8.19. Some time between the 07 and the 08 observations at Springfield, the temperature dropped by 7 °C and the pressure rose by nearly 4 hPa, signaling a strong cold frontal passage. The most pronounced shift in the wind (from SSW to WSW) did not occur at Springfield until the passage of the secondary cold front around 2 h later, between 09 and 10 UTC, and it was not until that time that the barometer began to rise unequivocally. The drop in temperature and dew point did not resume until between 11 and 12 UTC, when another much weaker rain band passed over the station. The narrow band of dry, subsiding air aloft was also passing over Springfield around 09 UTC (Fig. 8.18, middle).

The second radar image shown in Fig. 8.21, based on data taken about 9 h later, still exhibits a well-defined, narrow band of heavy rainfall that is virtually coincident with the position of the primary cold

[3] Squall lines are sometimes observed in the warm sector in advance of, and oriented parallel to, the cold front.

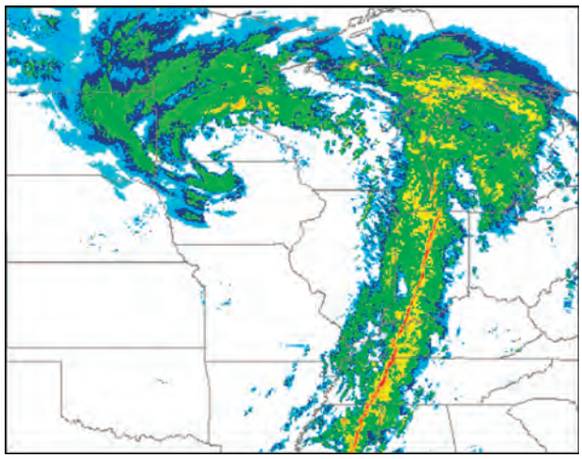

**Fig. 8.21** Composite radar image for 1535 UTC Nov. 10, 1998.

front. The major features in the distribution of radar echoes mirror the patterns in the 18 UTC satellite imagery, i.e., the comma-shaped cloud band emerging from the southern tip of the squall line and wrapping around the poleward flank of the cyclone and the slot of dry, relatively cloud-free air intruding from the west and wrapping around the equatorward and eastern flank of the cyclone. This "yin-yang"-like configuration is the signature of intertwined ascending and descending air currents in the vertical velocity field shown in the right-hand side of Fig. 8.5.

### 8.1.3 Vertical Structure

This subsection examines the vertical structure of this intense baroclinic wave using data formatted in three different ways: upper level charts at selected pressure levels, vertical soundings for selected radiosonde stations, and vertical cross sections.

#### *a. Upper level charts*

Figure 8.22 shows a series of upper level charts for 00 UTC Nov. 10, around the time when the associated extratropical cyclone was beginning to deepen rapidly. The corresponding sea level pressure and surface air temperature patterns have already been shown in Figs. 8.6 and 8.7. The 850-hPa height gradients tend to be stronger than the gradients in sea-level pressure (or 1000-hPa height) at the same location.[4] Stronger height gradients are indicative of higher geostrophic wind speeds. Comparing the numbers of wind barbs on the shafts in Figs. 8.6 and 8.22, it is evident that the actual winds are stronger at the 850-hPa level as well. Based on the thermal wind equation (7.20) we know that the strengthening of the westerly component of the wind from the surface to the 850-hPa level is consistent with the prevailing meridional temperature gradient in this layer, with colder air to the north. When the differences in contour intervals in the charts are taken into account, it is readily verified that the geopotential height gradients and wind speeds increase continuously with height up to the 250-hPa level, which corresponds to the level of the jet stream in Fig. 1.11. From 250 to 100 hPa, the highest level shown, the gradients and wind speeds decrease markedly with height.

The 850-hPa isotherms tend to be concentrated within the frontal zone extending from the Great Plains eastward to the Atlantic seaboard and passing through the surface low. To the east of the surface low, southerly winds are advecting the frontal zone northward, whereas to the south of the surface low, westerly winds are advecting it eastward. The frontal zone is particularly tight in the region of cold advection to the south of the surface low, and the temperature is remarkably uniform within a well-defined *warm sector* to the southeast of the surface low. The 850-hPa height contours that pass through the frontal zone exhibit strong cyclonic curvature.[5] Over the Carolinas the warm frontal zone on the 850-hPa chart is positioned quite far to the north of its counterpart on the surface charts. This northward displacement reflects the shallowness of the layer of trapped cool air to the east of the Appalachian mountain range.

Proceeding upward from the 850-hPa to the 250-hPa level, the patterns exhibit notable changes.

[4] From the hypsometric equation it is readily verified that the conventional 4-hPa contour interval for plotting sea-level pressure is roughly comparable to the 30-m contour interval used for plotting the 850-hPa height. Hence, the relative strength of the pressure gradient force (and the geostropic wind) at the two levels can be assessed qualitatively simply by comparing the spacing of the isobars and height contours.

[5] Frontal zones at any level are generally characterized by strong cyclonic vorticity. In stationary frontal zones the vorticity is manifested in the form of shear rather than curvature.

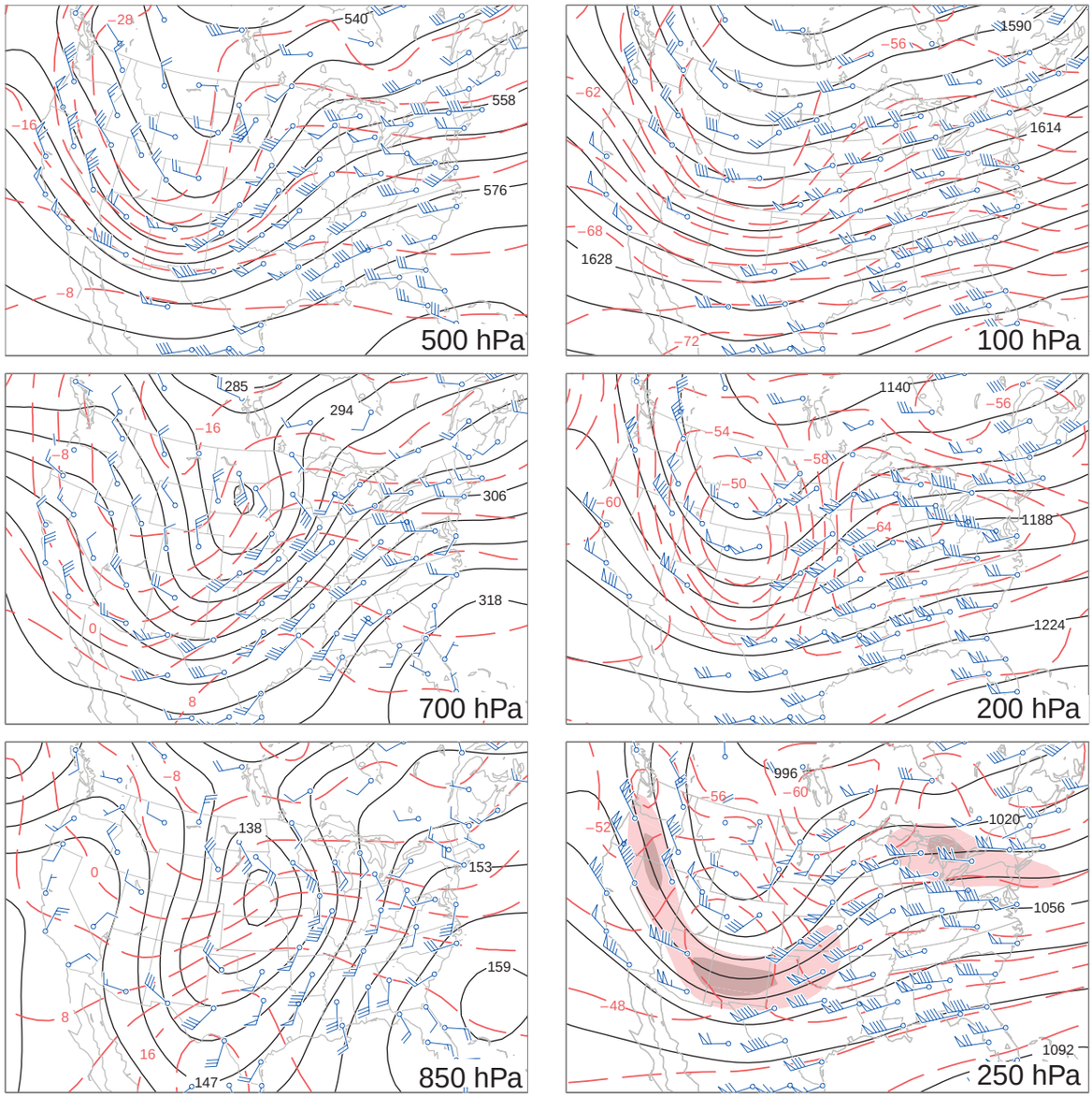


**Fig. 8.22** Upper level charts for 00 UTC Nov. 10, 1998, showing geopotential height (black contours), temperature (red contours), and observed winds. Contour interval 30 m for 850- and 700-hPa height, 60 m for 150-hPa height, 120 m for 250- and 200-hPa height, and 60 m for 100-hPa height. The contour interval for temperature is 4 °C in the left panels and 2 °C in the right panels. The shading in the 250-hPa chart are isotachs defining the position of the jet stream. Conventions for plotting wind vectors are shown in Fig. 8.1. [Courtesy of Jennifer Adams, COLA/IGES.]

As noted previously, the geopotential height gradients and the associated geostrophic winds generally increase with height[6] and this tendency is mirrored in the strength of the observed winds. The trough in the geopotential height field tilts westward with height by around 1/4 wavelength from the surface up to the 500-hPa level, but it exhibits relatively little vertical tilt above that level.

[6] In visually comparing the pressure gradients at the various levels, bear in mind that the contour interval doubles from the 700- to the 500-hPa level and doubles again from the 500- to the 250-hPa level.

The temperature contrast between the cold air mass over western Canada and the warm air mass over the subtropics gradually weakens with height. The orientation of the isotherms is much the same at the lowest three levels. Hence the expression of the baroclinic wave in the temperature field does not tilt westward with height. In most extratropical cyclones the baroclinic zones weaken and become progressively more diffuse as one ascends from the Earth's surface to the 500-hPa level. In this particular storm, the warm frontal zone weakens with height but the cold frontal zone remains quite strong up to the 500-hPa level. Upon close inspection it is evident that both warm and cold frontal zones slope backward toward the cold air with increasing height. The horizontal temperature advection within the frontal zones weakens with height as the wind vectors come into alignment with the isotherms. In contrast to the patterns at 850 and 700 hPa, which are highly baroclinic, the structure at the higher levels is more equivalent barotropic.

The temperature patterns in the lower stratosphere are weak and entirely different from those in the troposphere. At these levels (Fig. 8.22, right) the air in troughs in the geopotential height field tends to be warmer than the surrounding air, and the air in ridges tends to be cold. From the hypsometric equation it follows that the amplitudes of the ridges and troughs must decrease with height, consistent with the observations. By the time one reaches the 100-hPa level the only vestige of the baroclinic wave that remains is the weak trough over the western United States.

Now let us examine the structure of the tropopause in this high amplitude baroclinic wave. Vertical temperature profiles for stations in the trough and ridge of the wave are contrasted in Fig. 8.23. The profile for Denver, Colorado, which is located near the center of the 250-hPa trough, is relatively cold throughout the depth of the troposphere. The tropopause is marked by a sharp discontinuity in lapse rate around the 350-hPa (8 km) level, with a transition to more isothermal conditions above. In contrast, the profile for Davenport, Iowa, which is located in the 250-hPa ridge, exhibits a much colder and even sharper tropopause ~180 hPa (12.5 km). The tropopause temperature at this time was 20 °C colder at Davenport than at Denver. Stations such as Amarillo, Texas, which lie close to the axis of the jet stream, exhibit a more gradual decline in the lapse rate as one ascends from the troposphere into the stratosphere. The tropopause is not as well-defined in the Amarillo sounding as it is in the other two soundings.

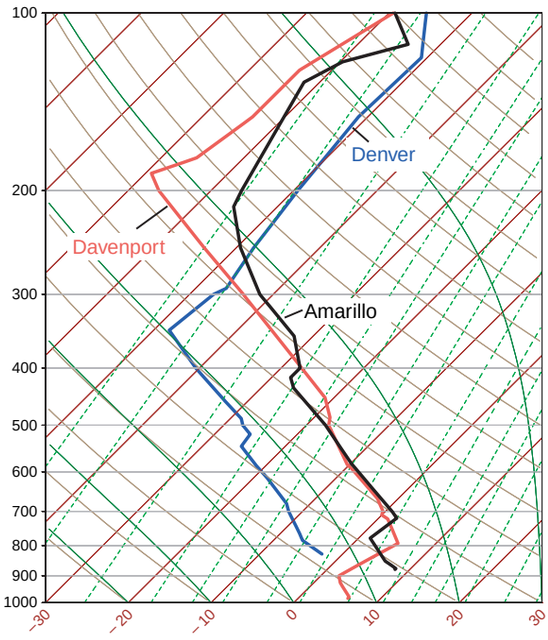


**Fig. 8.23** Vertical temperature soundings for Denver, Colorado (blue line), Amarillo, Texas (black line), and Davenport, Iowa (red line) at 00 UTC Nov. 10, 1998, plotted on a skew $T - \ln p$ diagram. [Courtesy of Jennifer Adams, COLA/IGES.]

Figure 8.24 shows how the tropopause structure relates to the lower tropospheric temperature

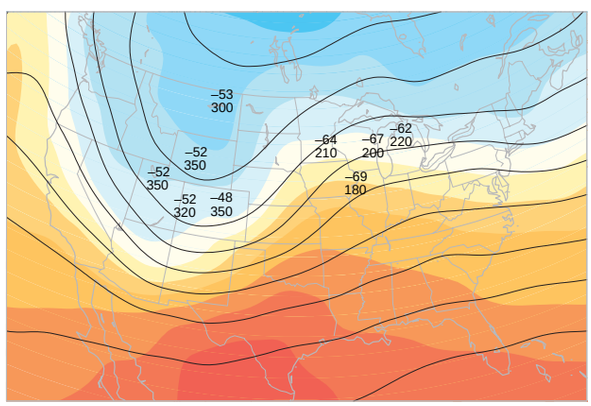


**Fig. 8.24** Height contours for the 250-hPa surface superimposed on 1000- to 500-hPa thickness (indicated by colored shading) as in Fig. 8.3 for 00 UTC Nov. 10, 1998. For selected stations, tropopause temperatures (TT in °C) and pressures (PPP in hPa) are plotted (TT/PPP). [Courtesy of Jennifer Adams, COLA/IGES.]

pattern and the flow at the jet stream level (250 hPa). The ridge and trough in the 250-hPa height pattern correspond, respectively, to the axes of the warmest and coldest air in the 1000- to 500-hPa thickness pattern, and the jet streams overlie the baroclinic zones, with colder air lying to the left. The depression of the tropopause in the vicinity of the 250-hPa trough, and directly above the cold air mass in the lower troposphere, is indicative of large-scale subsidence, as required by the continuity of mass [Eq. (7.39), Fig. 7.18]; i.e., as the cold air mass in the lower troposphere spreads out horizontally (as evidenced by the rapid advance of the surface cold front), the air above it must sink. The relatively high tropopause temperatures observed at stations deep within the cold air mass are due to the adiabatic warming of the subsiding air. At the 250-hPa level, relative humidities at these stations (not shown) were in the 25–40% range, consistent with a recent history of subsidence. In contrast, within the relatively warm, ascending air stream over the northern Great Plains, the tropopause is elevated; tropopause temperatures are relatively cold, and relative humidities are ~80%. Figure 8.24 also suggests a possible explanation of why the tropopause in the Amarillo sounding is not as clear as in the soundings for the other two stations shown in Fig. 8.23. Note that Amarillo lies along the axis of the jet stream, where the tropopause is like a vertical wall, with tropospheric air on the anticyclonic side and stratospheric air on the cyclonic side.

### b. Frontal soundings

This subsection examines vertical profiles of wind, temperature, and dew point in the lower troposphere at representative stations in different sectors of the developing cyclone. Soundings for two stations within the frontal zone are shown in Fig. 8.25. Amarillo lies within the segment of the frontal zone to the south of the surface low. In the Amarillo sounding the wind *backs* (i.e., turns cyclonically) with increasing height in the layer extending from the surface nearly up to the 700-hPa level. The backing is strongest in the inversion later extending from 780 to 720 hPa. Based on the thermal wind equation [Eq. (7.20)], backing implies cold advection. The layer of strong backing thus corresponds to the cold frontal zone and the cold front intersects the sounding at the top of the layer of strong backing at ~720 hPa. Davenport lies in an analogous position within the frontal zone to the east of the surface low, where the warm air is being advected northward by the southerly component of the wind. In the Davenport sounding the wind *veers* (turns anticyclonically) with increasing height, indicative of warm advection, from the surface up to 800 hPa, which marks the position of the warm front. In both the soundings shown in Fig. 8.25, the frontal zone corresponds to a layer of strong vertical wind

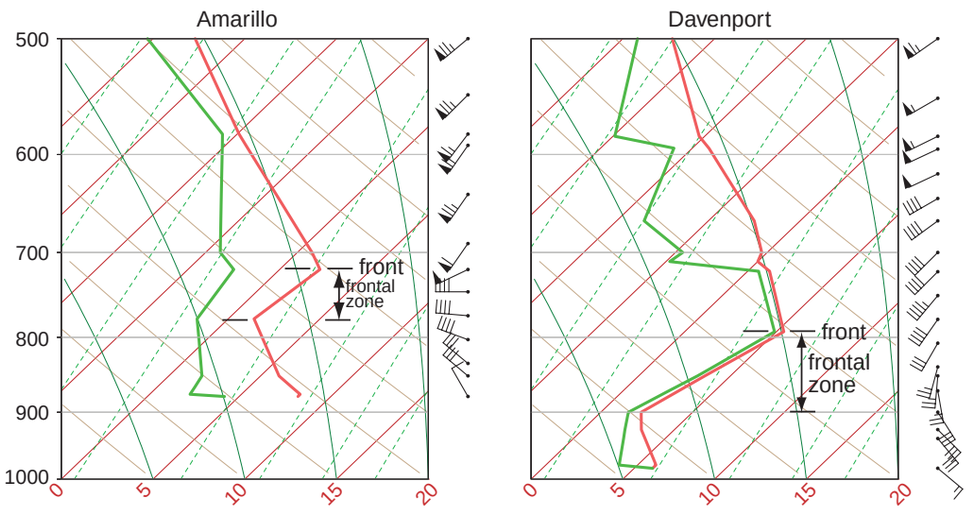


**Fig. 8.25** Soundings of wind, temperature (red lines), and dew point (green lines) at 00 UTC Nov. 10, 1998 at Amarillo, Texas (left) in the cold frontal zone and Davenport, Iowa (right) in the warm frontal zone. [Courtesy of Jennifer Adams, COLA/IGES.]

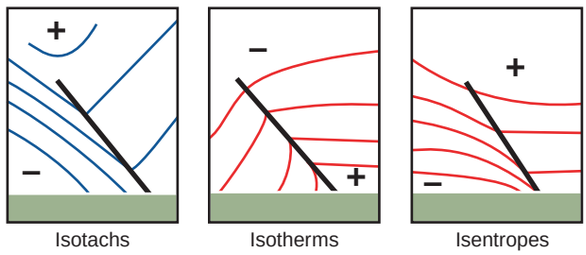


**Fig. 8.26** Idealized representations of a sloping frontal zone looking downwind at the jet stream level in the northern hemisphere (or upwind in the southern hemisphere). (Left) The wind component directed normal to the section: values into the section are denoted as positive. (Middle) Temperature. (Right) Potential temperature. Plus (+) and minus (−) signs indicate the polarity of the gradients (e.g., in the left the wind component into the section increases with height).

shear and high static stability, as evidenced by the presence of temperature inversions.

The idealized frontal cross sections shown in Fig. 8.26 are helpful in interpreting the frontal soundings. Consistent with the definition in Section 8.1.2b, at any given level the front marks the warm air boundary of the frontal zone. Consistent with Fig. 8.22, the front slopes backward, toward the colder air, with increasing height. Consistent with Fig. 8.25 the front marks the top of the frontal zone; it is characterized by high static stability and strong vertical wind shear. The frontal zone is depicted as being sharpest at the surface.

Soundings for stations located in the warm sector of the developing cyclone (not shown) exhibit little turning of wind with height other that the frictional veering just above the surface, and relatively little increase of wind speed with height. Stations in the cold sector to the west or northwest of the surface low exhibit relatively little turning of the wind with height, but in some storms they reverse direction, from northeasterly at low levels to southwesterly aloft.

### c. Vertical cross sections

Vertical cross sections are the natural complement to horizontal maps in revealing the three-dimensional structure of weather systems. A generation ago, the construction of cross sections was a labor-intensive process that involved blending temperatures and geostrophic winds derived from constant pressure charts with wind and temperature data for intermediate levels extracted from soundings for stations lying along the section. Interpolating fields in the gaping holes between data points could be a formidable challenge, even for the skilled analyst. With today's high-resolution gridded data sets generated by sophisticated data assimilation schemes, all the analyst need do to generate a section is to specify the time and orientation and the fields to be included.

The two most widely used variables in vertical cross sections are temperature (or potential temperature) and geostrophic wind. The sections are usually oriented normal to the jet stream in which case, isotachs of the wind component normal to (or through) the section reveal the location and strength of the jet stream where it passes through the plane of the section, and they often capture the zones of strongest vertical wind shear, where patches of clear air turbulence tend to be concentrated. If the flow through the section is not strongly curved, then the vertical shear of the geostrophic wind component normal to the section and the horizontal temperature gradient along the section are approximately related by the thermal wind equation

$$\frac{\partial V_{gn}}{\partial p} \simeq -\frac{R}{fp}\frac{\partial T_n}{\partial s} \tag{8.1}$$

where $V_{gn}$ is the geostrophic wind component into the section and $T_n$ is temperature in the plane of the section, with the horizontal coordinate $s$ defined as increasing toward the right. Hence, at any point in the section the horizontal temperature gradient is directly proportional to the vertical wind shear. It follows that the horizontal spacing of the isotherms is directly proportional to the vertical spacing of the isotachs plotted in the section. For example, in regions of the section in which the flow is barotropic, the isotherms (or isentropes) are horizontal (i.e., $\partial T/\partial s = 0$) and the isotachs are vertical (i.e., $\partial V_{gn}/\partial p = 0$). These conditions also apply locally in the core of a jet stream. Near the tropopause, the vertical wind shear and the horizontal temperature gradient both undergo a sign reversal at the same level, at which point the isotachs are vertical and the isotherms are horizontal.

The same relationships apply to vertical wind shear and the horizontal gradient of potential temperature. Vertical cross sections for temperature and potential temperature tend to be somewhat different in appearance because temperature in the troposphere usually decreases with height, whereas potential temperature increases with height, and in the stratosphere $\partial\theta/\partial p$ is always strong and negative, whereas $\partial T/\partial p$ is often weak and may be of either sign.

Another variable that is frequently plotted in vertical cross sections is isentropic potential vorticity,

$$\mathrm{PV} \equiv -g\,(\zeta_\theta + f)\,\frac{\partial\theta}{\partial p} \qquad (8.2)$$

as defined in Section 7.2.10. PV is a conservative tracer that serves as a marker for intrusions of stratospheric air into the troposphere in the vicinity of the jet stream. Air that has resided in the stratosphere for any appreciable length of time acquires high values of static stability $-\partial\theta/\partial p$ by virtue of the vertical gradient of diabatic heating at those levels. Hence, the potential vorticity of stratospheric air tends to be much higher than that of tropospheric air. When a layer of stratospheric air is drawn downward into the troposphere, columns are stretched in the vertical, pulling the potential temperature surfaces apart, thereby causing the static stability to decrease. Conservation of potential vorticity requires that the vorticity of the air within the layer becomes more cyclonic as it is stretched in the vertical.

Now let us consider two examples of vertical cross sections. The first example, shown in Fig. 8.27, is oriented perpendicular to the cold front and jet stream over the southern Great Plains at 00 UTC. The viewer is looking downstream (i.e., northeastward): the colder air is toward the left. In denoting positions along the section, we will be referring to a series of imaginary stations, indicated by letters A, B . . . etc. along the baseline of the section. The front at the Earth's surface is at C and the frontal zone is apparent to the west of station C as a wedge of sloping isotherms (i.e., the red contours) and strong vertical wind shear, as indicated by the close spacing of the isotachs (blue contours) in the vertical. Consistent with the idealized depictions in Fig. 8.26, the front (i.e., the warm air boundary of the frontal zone) slopes backward, toward the cold air, with increasing height. The front becomes less clearly defined at levels above 700 hPa. The jet stream with a maximum wind speed of nearly 50 m s$^{-1}$ passes through the section above station C at the 250-hPa level.

The tropopause is clearly evident in Fig. 8.27 as a discontinuity in the vertical spacing of the isotherms: in the troposphere the isotherms are closely spaced in the vertical, indicative of strong lapse rates, while in the stratosphere, they are widely spaced, indicative of nearly isothermal lapse rates. Consistent with Fig. 8.24, the tropopause is low and relatively warm on the cyclonic (left) side of the jet stream and high

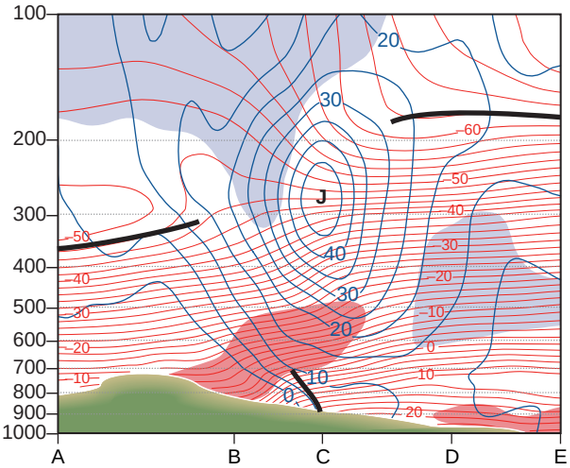


**Fig. 8.27** Vertical cross section of wind and temperature for 00 UTC Nov. 10, 1998. This section extends from Riverton, Wyoming to Lake Charles, Louisiana (KRIW to KLCH; see Fig. 8.36). Temperature is indicated by red contours, and isotachs of geostrophic wind speed normal to the section, with positive values defined as southwesterly winds directed into the section, are plotted in blue. Regions with relative humidities in excess of 80% are shaded in red and below 20% in blue. Heavy black lines indicate positions of the surface-based fronts and the tropopause. The orientation of the section relative to the front is indicated in Fig. 8.36 at the end of this section. [Courtesy of Jennifer Adams, COLA/IGES.]

and cold on the anticyclonic (right) side. An aircraft flying along the section at the jet stream (250-hPa) level, passing from the warm side to the cold side of the lower tropospheric frontal zone, would pass from the upper troposphere to the lower stratosphere while crossing the jet stream. Entry into the stratosphere would be marked by a sharp decrease in relative humidity and an increase in the mixing ratio of ozone. One would also observe a marked increase in the PV of the ambient air: a consequence of both the increase in static stability $-\partial\theta/\partial p$ (i.e., compare the lapse rates at the 250-hPa level at stations D and B) in combination with a transition from weak anticyclonic (negative) relative vorticity $\zeta$ on the equatorward flank of the jet stream to quite strong cyclonic (positive) relative vorticity on the poleward flank.

Figure 8.28 shows a vertical cross section normal to the frontal zone 12 h later. In this section the red contours are isentropes (rather than isotherms), and high values of PV, indicative of stratospheric air, are indicated by shading. The jet stream is stronger in this section than in the previous one, with peak wind speeds of ~60 m s$^{-1}$. Immediately beneath the jet

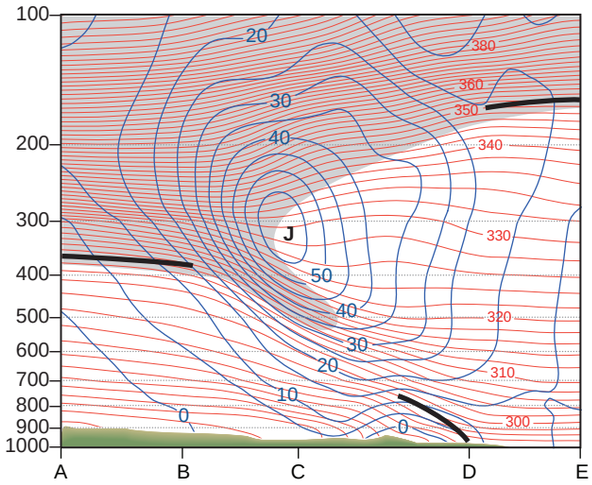


**Fig. 8.28** Vertical cross section of wind and potential temperature for 12 UTC Nov. 10, 1998. This section extends from North Platte, Nebraska to Jackson, Mississippi (KLBF to KJAN; see Fig. 8.36). Potential temperature is indicated by red contours, and isotachs of geostrophic wind speed normal to the section are plotted in blue with positive values defined as southwesterly winds directed into the section. The region in which isentropic potential vorticity exceeds $10^{-6}$ K m$^2$ s$^{-1}$ kg$^{-1}$ is indicated by shading. Heavy black lines represent the position of the surface-based fronts and tropopause. [Courtesy of Jennifer Adams, COLA/IGES.]

stream is a layer characterized by very strong vertical wind shear. Consistent with the thermal wind equation, the temperature gradient in this layer is very strong, with colder air to the left. The air within this *upper level frontal zone* exhibits strong cyclonic relative vorticity by virtue of its cyclonic shear $\partial V_n/\partial s$ and is also characterized by strong static stability, as evidenced by the tight vertical spacing of the isentropes. It follows that the PV of the air within this upper level frontal zone is much higher than that of typical air parcels at this level and the air within the core of the jet stream. Accordingly, the PV contours are folded backward beneath the jet stream so as to include the upper tropospheric frontal zone within the region of high PV. Since the PV contours define the boundary between tropospheric air and stratospheric air, it follows that the air within the upper part of the frontal zone is of recent stratospheric origin.

Such upper level frontal zones and their associated *tropopause folds* are indicative of extrusions of stratospheric air, with high concentrations of ozone and other stratospheric tracers, into the upper troposphere. Sometimes tropopause folding is a reversible process in which the high PV air within the fold is eventually drawn back into the stratosphere. At other times the process is irreversible: the extruded stratospheric air becomes incorporated into the troposphere, where it eventually loses its distinctively high PV. The extrusion in Fig. 8.28 was evident 12 h earlier in north–south sections through the core of the jet stream over New Mexico, where the jet stream was strongest at that time. With the development of the cyclone, the stratospheric air was drawn downward and northeastward over the cold frontal zone, becoming an integral part of the "dry slot" in the water vapor satellite imagery (Fig. 8.18). The resulting injection of air with high PV into the environment of the cyclone contributed to the remarkable intensification of this system during the later stages of its development.

### 8.1.4 Air Trajectories

This subsection provides a *Lagrangian* perspective on extratropical cyclones. Lagrangian trajectories are constructed from three-dimensional velocity fields at several successive times separated by an interval of a few hours. The trajectories can either be tracked forward in time from prescribed positions at some initial time $t_0$ or can be tracked backward in time from prescribed positions at a final time $t_f$. Since convective motions are not explicitly represented in the synoptic charts, their role in the vertical transport of air parcels must either be ignored, or parameterized in some way.

Figure 8.29 shows a set of trajectories whose end points lie within the cloud shield of a mature extratropical storm. Air parcels ascending along trajectories like these supply most of the moisture that falls as rain and snow in these storms. The trajectories are depicted in coordinates moving northeastward with the center of the surface low, where the coordinate transformation is accomplished by subtracting out the movement of the surface low from the horizontal velocity in each time step of the trajectory calculation. Air parcels such as A that make up the eastern part of the cloud shield can be traced back to low levels in the warm sector of the cyclone; those such as B and C that comprise the northern flank came from the warm frontal zone farther to the north and east. The anticyclonic curvature of trajectories A, B, and C is a consequence of the veering of the wind with height in the region of warm geostrophic temperature advection in advance of the surface low.

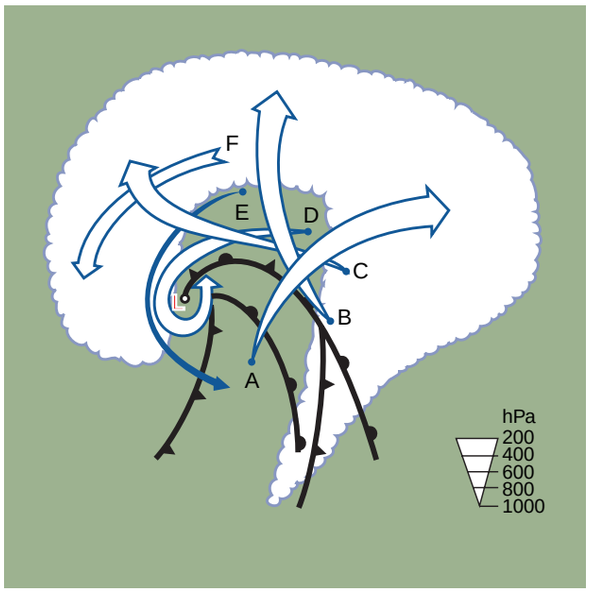


**Fig. 8.29** Family of three-dimensional trajectories in an intense extratropical cyclone, as inferred from a high-resolution grid point dataset for an actual storm over the North Atlantic. The trajectories are shown in a coordinate system moving with the cyclone. Two different frontal positions are shown: the lower one is for an earlier time when the configuration is that of an open wave and the upper one is for a later time when the cyclone is in its mature stage and exhibits an occluded front. The configuration of the cloud shield and the position of the surface low correspond to the later time. The width of the arrows gives an indication of the height of the air parcel in accordance with the scale at the lower right. [Adapted from *Mon. Wea. Rev.*, **120** (1995) p. 2295.]

Trajectories D, E, and F are a bit more complicated. D starts out in the warm frontal zone, ascends, and becomes saturated as it circulates around the rear of the surface low within the inner part of the cloud shield. Trajectory D subsequently descends and becomes unsaturated as it recurves northward behind the occluded front. Trajectory E does not ascend appreciably: it passes underneath the head of the comma-shaped feature and into the rear flank of the cold frontal zone. The comma-shaped feature on the western side of the cloud shield is made up of parcels with trajectories such as F, which can be traced back midlevels in the cold air mass to the north of the storm.

Hence, the ascending trajectories describe a fan-like spreading of the rising air. The rising air parcels exhibit a continuum of equivalent potential temperatures, with that for the southernmost trajectory A being highest and those B–F being progressively lower. Wherever the trajectories that start out at the surface cross, the colder one passes beneath the warmer one.

Figure 8.30 shows a bundle of descending trajectories in the cloud-free region to the rear of the cyclone. These air parcels can be traced back to the northwesterly flow in the vicinity of the jet stream level behind the trough of the wave. The trajectories start out vertically stacked and spread out as they descend behind the cold front, with the air parcels warming at a rate close to the dry adiabatic lapse rate. The fan-shaped surface formed by the spreading trajectories slopes upward toward the north. The air parcels that started near the top of the bundle curve cyclonically around the surface low, forming the "dry slot" at the northern part of the fan-shaped surface. The trajectories in the dry slot do not descend all the way to the Earth's surface: they typically level off as they pass over the occluded front and begin to ascend as they approach the cloud shield to the north. However, they are so dry that they remain unsaturated as they cross over the top of the cloud shield.

The air parcels that started near the bottom of the bundle at the jet stream level curve anticyclonically around the surface high, forming the southern part of the fan-shaped surface depicted in Fig. 8.30. The trajectories on this side of the surface descend low

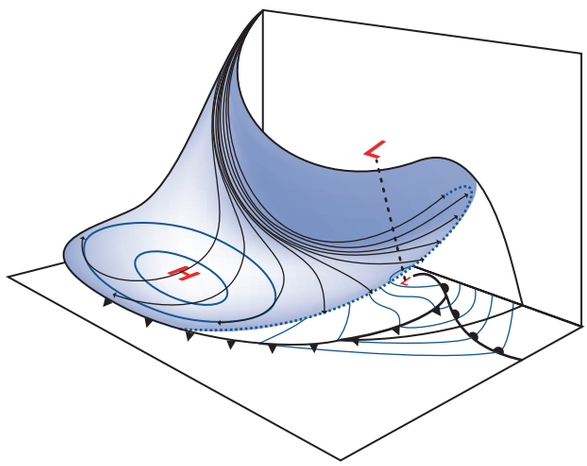


**Fig. 8.30** Idealized 24-h trajectories for selected air parcels in the descending branch of an intense extratropical cyclone similar to the one examined in the case study in this section. The trajectories start and end at about the same time. Black arrows are the trajectories and blue contours are isobars of sea-level pressure. [From Project Springfield Report, U.S. Defense Atomic Support Agency, NTIS 607980 (1964).]

enough so that parcels may be entrained into the boundary layer of the modified polar air mass advancing southward behind the cold front. If a pronounced tropopause fold is present at the upstream end of the trajectories at the jet stream level, stratospheric air may be entrained into this anticyclonic air stream. Such relatively rare and brief incursions of stratospheric air into the boundary layer are marked by extremely low relative humidities and high ozone concentrations in surface air.

### 8.1.5 In Search of the Perfect Storm

For nearly a century meteorologists have argued about what constitutes "the perfect storm": "perfect," not in the sense of most catastrophic, but most typical of the cyclones generated by baroclinic instability in the real atmosphere. The case study featured in this section conforms in most respects to the classical *Norwegian polar front cyclone model* devised by J. Bjerknes and collaborators of the Bergen School during the 1920s for interpreting surface weather observations over the eastern North Atlantic and Europe. Characteristic features of the archetypical Norwegian polar front cyclone, summarized in Fig. 8.31, include the strong cold front, the weaker occluded front, and the comma-shaped cloud shield.

Some of the most intense cyclones that develop over the oceans during wintertime exhibit significant departures from this well established paradigm. Their spiral cloud bands, as revealed by satellite imagery, are coiled up more tightly about the center of the surface low than the cloud shield in our case study: see, for example, Fig. 1.12. Unlike the storm in the case study, mature cyclones that exhibit this tightly coiled structure tend to be *warm core*: i.e., the air in the center of the surface low is warmer than the surrounding air on all sides.

Figure 8.32 shows an idealized schematic of the structure and evolution of these tightly coiled storms, as deduced from data from instrumented aircraft flying through them at low levels, as well as numerical simulations with high resolution models based on the primitive equations. The four cyclones represent snapshots of a single cyclone at successive stages of its life cycle as it evolves from a weak frontal wave in (I) to a fully developed cyclone in (IV).

In the early stages of development (I and II) the configuration of the fronts and isotherms resembles the classical, Norwegian polar front cyclone model, with warm and cold fronts beginning to circulate around the center of a deepening low pressure center. The only perceptible difference is the pronounced cyclonic shear of the flow and the relatively greater prominence of the warm front. As the development

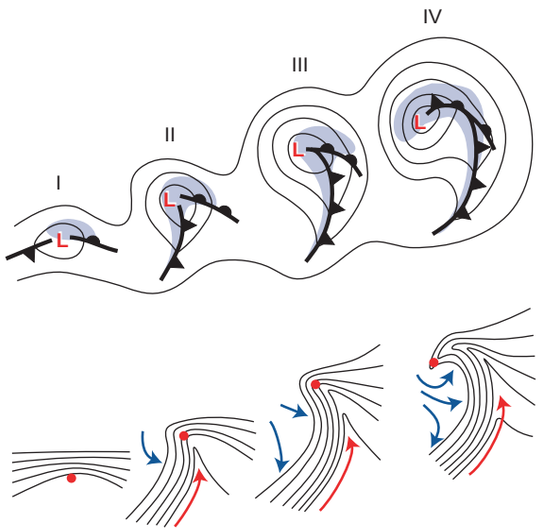


**Fig. 8.31** Schematic showing four stages in the development of extratropical cyclones as envisioned in the Norwegian polar front cyclone model. Panels I, II, III and IV represent four successive stages in the life cycle. (Top) Idealized frontal configurations and isobars. Shading denotes regions of precipitation. (Bottom) Isotherms (black) and airflow (colored arrows) relative to the moving cyclone center (red dot). Red arrows indicate the flow in the warm sector, and blue arrows indicate the flow in the cold air mass. Frontal symbols are listed in Table 7.1. [Adapted from *Mon. Wea. Rev.*, **126** (1998) p. 1787.]

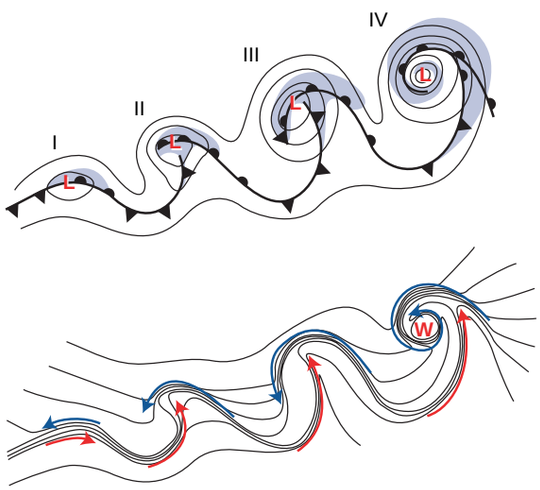


**Fig. 8.32** As in Fig. 8.31 but for tightly coiled, warm core storms. [From *Extratropical Cyclones: The Erik Palmén Memorial Volume*, Amer. Meteorol. Soc. (1990) p. 188.]

proceeds, the warm frontal zone continues to sharpen and bridges across the poleward side of the surface low. This zone of sharp thermal contrast maintains its identity as it is advected around the back side of the low in stage III and coiled into a tight, mesoscale spiral in stage IV. This extension of the warm front is sometimes referred to as a *bent back warm occlusion*. This segment of the front is occluded in the sense that the air on the warm side of the frontal zone cannot be traced back to the warm sector of the storm. In this case the label *warm* derives not from the direction of movement, but from the frontal history; depending on the rate of movement of the storm and the direction of the observer relative to the low pressure center, the front may be moving in either direction.

Throughout the development process, the cold frontal zone is less pronounced than the warm frontal zone and the innermost part of it actually weakens as the storm begins to take shape. At stage III, the weakening inner segment of the cold front intersects the stronger warm front at right angles, creating a configuration reminiscent of a T-bone steak. The cold front advances eastward more rapidly than the center of the cyclone and becomes separated from it in stages III and IV.

Cold air spiraling inward along the outer side of the warm front, indicated by the blue arrows in Fig. 8.32, encircles and secludes the relatively warm air in the center of the cyclone, creating the mesoscale warm core. The strongest inflow of warm air, indicated by the red arrow, occurs just ahead of the cold front. Bands of cloudiness and precipitation tend to be located ahead of the cyclonically circulating warm and cold fronts, while drier, relatively cloud-free air spirals inward behind the cold front.

Consistent with the thermal wind equation (as generalized to the gradient wind) the tight cyclonic circulation around the center of the storm weakens rapidly with height above the top of the boundary layer. The wraparound warm front slopes outward, toward the colder air, with increasing height and it diminishes in intensity. Hence, the mesoscale warm air seclusion at the center of the cyclone expands with increasing height, but it also diminishes in intensity.

In the atmospheric dynamics literature, tightly coiled, warm core cyclones are referred to as LC1 storms and cyclones that conform to the Norwegian model as LC2 storms (where LC stands for life cycle). A third category LC3 refers to *open wave cyclones* (i.e., cyclones that never develop occluded fronts) in which the cold front is dominant. One can conceive of an archetypal (or "perfect") storm for each of these three models.

Numerical simulations in which baroclinic waves are allowed to develop on various background flows offer insights as to what conditions favor the development of cyclones that conform to the Norwegian polar front cyclone model versus the tighter, more axially symmetric, warm core cyclones exemplified by Figs. 1.12 and 8.32. The determining factors appear to be the barotropic shear and confluence/diffluence of the background flow.

The three kinds of cyclones (LC1, LC2, and LC3) are different outcomes of the same instability mechanism: baroclinic instability, which can occur even in a dry atmosphere. All three involve the amplification of a wave in the temperature field by horizontal temperature advection and the release of potential energy by the sinking of colder air and the rising of warmer air. In all three, the rising and sinking air flows and their attendant fronts spiral inward toward the center of the cyclone. Even their frontal structures are similar in many respects.

### 8.1.6 Top–Down Influences

In numerical simulations of baroclinic waves developing on a pure zonal background flow, the disturbances reach their peak amplitude first in the lower troposphere, and a day or so later at the jet stream level. In nature, cyclone development (*cyclogenesis*) is almost always "top-down"; it is initiated and subsequently influenced by dynamical processes in the upper troposphere. To generate a cyclone as intense as the one examined in the case study, conditions in the upper and lower troposphere must both be favorable.

The region of cyclonic vorticity (and potential vorticity) advection downstream of a strong westerly jet is a favored site for cyclogenesis, especially if such a feature passes over a preexisting region of strong low level baroclinicity (e.g., the poleward edge of a warm ocean current, the ice edge, or a weakening frontal zone left behind by the previous storm). Extrusions of stratospheric air, with its high potential vorticity, into frontal zones at the jet stream level can increase the rate of intensification of the cyclonic circulation in the lower troposphere.

Extratropical cyclones sometimes occur in association with long-lived *baroclinic wave packets*, which are more clearly evident at the jet stream level

than down at the Earth's surface. The existence and behavior of wave packets are illustrated by the time-longitude plot of the meridional wind component at the jet stream level shown in Fig. 8.33. The pervasive wave-like signature, with a wavelength of around 50° of longitude (~4000 km on the 45 °N latitude circle) is the signature of baroclinic waves. That the individual maxima and minima slope toward the right as one proceeds downward in the diagram is evidence of eastward phase propagation. The average phase speed of the waves in this plot is 7° of longitude per day (6 m $s^{-1}$). Envelopes comprising several successive waves sectors in which the wave amplitude is relatively large are referred to as *wave packets*. For example, on November 14 a wave packet is passing over the Atlantic sector. Upon close inspection, it is evident that the wave packets propagate eastward with time with a speed of nearly 20 m $s^{-1}$, three times the phase speed of the individual waves embedded within the packets. New waves are continually developing downstream of a wave packet, while mature waves are dying out at the upstream end of it: hence the lifetime of a wave packet transcends the lifetimes of the individual waves of which it is comprised.

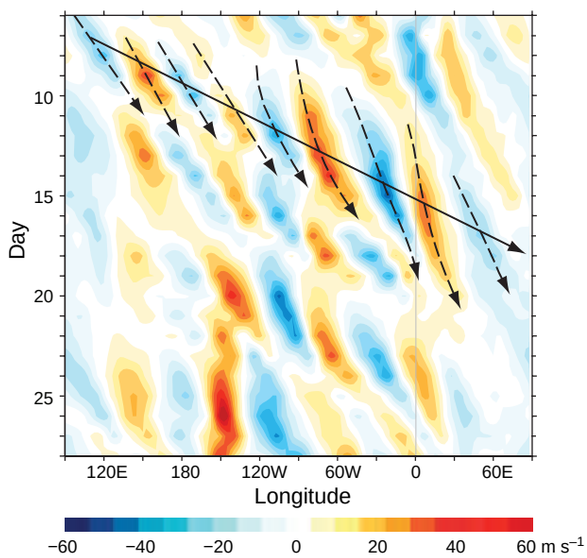


**Fig. 8.33** Time-longitude section of the 250-hPa meridional wind component (in m $s^{-1}$) averaged from 35 °N to 60 °N for November 6–28, 2002, a period marked by well-defined baroclinic wave packets and several major northern hemisphere cyclogenesis events. Slopes of the dashed arrows indicate the phase velocities of the waves, and the solid arrow indicates the group velocity of the wave packets. [Courtesy of Ioana Dima.]

The observed tendency for *downstream development* of wave packets is a consequence of the dispersive character of Rossby waves (i.e., the fact that their speed of propagation is a function of their wavelength). The rate of propagation of the packets is closely related to the group velocity of Rossby waves.[7]

### 8.1.7 Influence of Latent Heat Release

Another factor that contributes to the vigor and diversity of extratropical cyclones is the release of latent heat of condensation in regions of precipitation. Because latent heat release occurs preferentially in warm, rising air masses, it acts to maintain the horizontal temperature gradients within the storm, thereby increasing the supply of potential energy available for conversion to kinetic energy. Numerical simulations of cyclogenesis with and without the inclusion of latent heat release confirm that precipitating storms tend to deepen more rapidly and achieve greater intensities than storms in a dry atmosphere.

Precipitation in extratropical cyclones is often widespread but inhomogeneous in space and time, with much of it concentrated within elongated mesoscale *rain bands* with areas ranging from $10^3$ to $10^4$ $km^2$ and with lifetimes of several hours. The axes of the rain bands tend to be aligned with the low level isotherms which, in turn, tend to be aligned with the vertical wind shear and with the fronts, as depicted in Fig. 8.34. The bands that lie along the fronts are fed by ascending air trajectories along the frontal surface, as depicted in Fig. 8.9. Pre- and postfrontal rain bands are the manifestations of instabilities within the broad deformation zone that lead to locally enhanced baroclinicity and upward motion.

Within the rain bands are smaller ($10^2$ to $10^3$ $km^2$) mesoscale regions in which the precipitation rates are further enhanced by the presence of convective cells, as explained in more detail in the next section. The lifting that occurs in association with a cold front advancing into a warm, humid, convectively unstable air mass can give rise to a line of convective cells forming an intense, narrow

[7] See J. R. Holton, *Dynamic Meteorology*, 4th edition. Academic Press (2004) pp. 185–188.

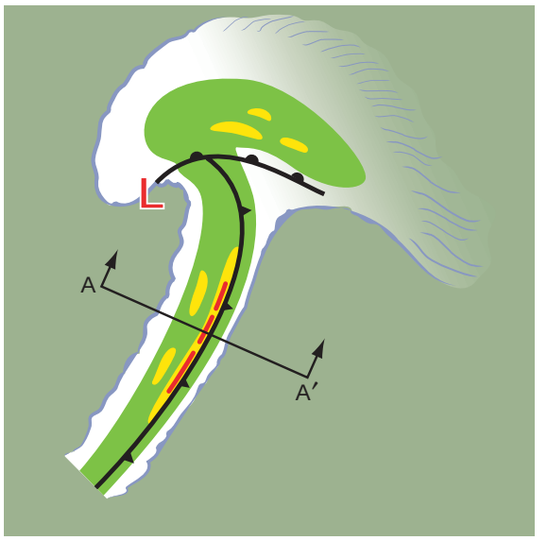


**Fig. 8.34** Idealized schematic emphasizing the kinds of mesoscale rain bands frequently observed in association with a mature extratropical cyclone. The green shading within the cloud shield denotes light precipitation, yellow shading denotes moderate precipitation, and red shading denotes heavy precipitation. [Courtesy of Robert A. Houze.]

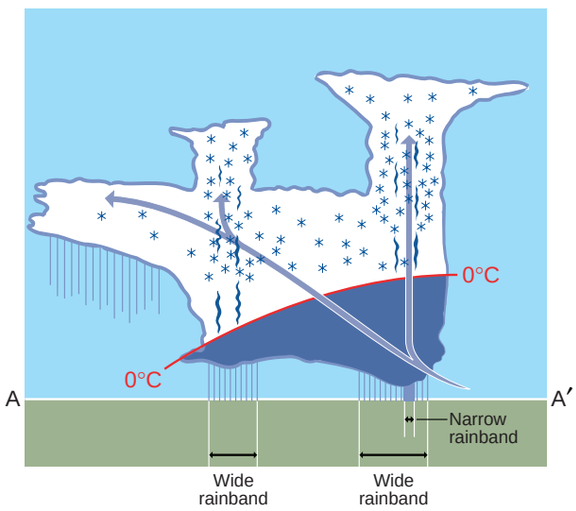


**Fig. 8.35** Vertical cross section along AA′ in Fig. 8.34. The position of the cold front at the Earth's surface coincides with the leading edge of the narrow cold frontal rainband, and the frontal surface tilts upward toward the west with a slope comparable to that of the air trajectory. The dark blue shading indicates areas of high liquid water concentration, and the density of the blue asterisks is proportional to the local concentration of ice particles. High liquid water contents are restricted to the layer below the 0 °C isotherm except in regions of strong updrafts in convective cells, as represented by the narrow, dark blue "chimneys." See text for further explanation. [Adapted from *Cloud Dynamics*, R. A. Houze, p. 480, Copyright (1993), with permission from Elsevier.]

cold-frontal rainband, like the ones shown in Figs. 8.19 and 8.21. A vertical cross section through a complex of cold frontal rain bands is shown in Fig. 8.35. The wide frontal and postfrontal rain bands are a consequence of convective cells embedded within the broader rain area. Updrafts in the cells carry cloud liquid water well above the freezing level, where it quickly condenses onto ice particles, enabling them to grow rapidly to a size at which they fall to the ground, enhancing the rainfall rate. The narrow cold frontal rainband coincides with a line of particularly intense convective cells fueled by the lifting action of the front.

Vigorous convective features such as squall lines can sometimes take on a life of their own, modifying the structure of the extratropical cyclones in which they are embedded. Under these conditions, rainfall patterns may depart substantially from those typically associated with baroclinic waves and the frontal configuration may even be modified. Deep convection plays a particularly important role during the warm season, when the equator-to-pole temperature gradient is relatively weak and rainfall rates can be very high.


**Fig. 8.36** Locations of the stations and vertical cross sections shown in this section. From north to south, KMQT is the station identifier for Marquette, Michigan; KRIW for Riverton, Wyoming; KLBF for North Platte, Nebraska; KSUX for Sioux Falls, South Dakota; KGAG for Gage, Oklahoma; KSGF for Springfield, Missouri; KBWG for Bowling Green, Kentucky; KCAE for Columbia, South Carolina; KJAN for Jackson, Mississippi; and KLCH for Lake Charles, Louisiana.